# 1 Countrywide Digital Surface Models and Vegetation Height Models

## 2 from Historical Aerial Images

- 3 Mauro Marty<sup>1</sup>, Livia Piermattei<sup>1,2</sup>, Lars T. Waser<sup>1</sup>, Christian Ginzler<sup>1</sup>
- <sup>4</sup> Land Change Science Research Unit, Swiss Federal Institute for Forest, Snow and Landscape Research WSL, Birmensdorf,
- 5 8903, Switzerland
- 6 <sup>2</sup>Department of Geography, University of Zurich, Zurich, 8057, Switzerland
- 7 Correspondence to: Mauro Marty (mauro.marty@wsl.ch)
- 8 **Abstract.** Historical aerial images, captured by film cameras in the previous century, are valuable resources for quantifying
- 9 Earth's surface and landscape changes over time. In the post-war period, these images were often acquired to create
- 10 topographic maps, resulting in the acquisition of large-scale aerial photographs with stereo coverage. Photogrammetric
- techniques applied to these stereo images enable the extraction of 3D information to reconstruct digital surface models (DSMs)
- 12 and orthoimages.
- Here, we present a highly automated photogrammetric approach for generating countrywide DSMs of Switzerland, at a 1 m
- resolution, from approximately 32,000 scanned aerial stereo images acquired between 1979 and 2006, with known exterior
- and interior orientation. We derived four countrywide DSMs for the epochs 1979–1985, 1985–1991, 1991–1998, and 1998–
- 16 2006. From the DSMs, we generated corresponding countrywide vegetation height models (VHMs). We assessed the quality
- 17 of the historical DSMs at the country scale and within six representative study sites, evaluating the vertical accuracy and the
- completeness of image-matching across different land cover types.
- Mean completeness ranged from 64% for 'glacial and perpetual snow' to 98% for 'sealed surfaces', with a value of 93% for
- 20 the 'closed forest' class. Across Switzerland, the median elevation accuracy of the historical DSMs compared with a reference
- digital terrain model (DTM) on sealed surface points ranged from 0.08 to 0.16 m, with a normalised median absolute deviation
- 22 (NMAD) of around 0.8 m and a maximum root mean square error (RMSE) of 1.20 m. Similar accuracies are obtained when
- comparing historical DSMs with measured geodetic points.
- 24 The VHMs generated in this study enabled the detection of major changes in forest areas due to windstorm damage, forest
- 25 dynamics, and growth. This work demonstrates the feasibility of generating accurate, very high-resolution DSM time series
- 26 (spanning three decades) and VHMs from historical aerial images of the entire surface of Switzerland in a highly automated
- 27 manner. The VHMs are already being used to estimate countrywide biomass changes. The countrywide DSMs and VHMs for
- the four epochs, along with auxiliary data, are available online at <a href="https://doi.org/10.16904/envidat.528">https://doi.org/10.16904/envidat.528</a> (Marty et al., 2024) and
- 29 can be used to quantify long-term elevation changes and related processes across different surfaces.

#### 1 Introduction

- 31 Photographs taken by film cameras on aeroplanes throughout the last century represent a unique and invaluable information
- 32 source for quantifying past changes in the Earth's surface and landscape. Various institutions and mapping agencies have
- 33 recognised this value by preserving and scanning these photographs and making them publicly available.
- 34 After the Second World War, large-scale aerial photographs were frequently taken to create topographic maps. To ensure
- 35 stereoscopic coverage and enable the extraction of three-dimensional (3D) information, image blocks were acquired in parallel
- 36 strips, with each photograph overlapping the next along the same flight line (forming a stereo pair). Due to the stereoscopic
- 37 acquisition and very high resolution of these images, digital surface models (DSMs) and orthoimages at a metric or sub-metric
- 38 resolution can be generated using digital photogrammetry and computer vision techniques. This capability has led to the use
- 39 of historical aerial images to assess long-term surface elevation changes across various geoscience fields.
- 40 Multi-temporal DSMs derived from historical aerial images have frequently been used in cryospheric research for assessments
- 41 of changes in glacier elevation (e.g., Magnússon et al., 2016; Belart et al., 2020; Denzinger et al., 2021), in periglacial studies
- 42 (e.g., Cusicanqui et al., 2021; Fleischer et al., 2021), in geomorphology (e.g., Micheletti et al., 2015; Piermattei et al., 2023;
- 43 Schwat et al., 2023), in volcanology (e.g., Gomez et al., 2015), in analyses of land-use change (e.g., Nebiker et al., 2014; Bolles
- et al., 2018) and in archaeology (e.g., Risbøl et al., 2015; Peppa et al., 2018). Most studies have been focused on local scales
- 45 and have involved processing a small set of scanned aerial images, with a few considering larger scales (Geyman et al., 2022;
- 46 Muhammed et al., 2023) or even regional scales such as Greenland (Korsgaard et al., 2016).
- 47 In this study, we generated countrywide DSMs of Switzerland using historical aerial images acquired from the 1980s to the
- 48 early 2000s. Additionally, as we carried out the study within the framework of the Swiss National Forest Inventory (NFI), we
- 49 produced corresponding countrywide vegetation height models (VHMs). The Swiss NFI aims to collect objective information
- on forests at the national level for scientific, political, social and economic purposes (Abegg et al., 2023). Data collection
- 51 within the context of the NFI is mainly based on a systematic terrestrial sample inventory, which is intended to provide results
- 52 for Switzerland as a whole, as well as for larger regions and individual cantons. Since the early days of the NFI, aerial image
- 53 interpretation and remote sensing data have been used. Over the decades, the image data has evolved from analogue black-
- 54 and-white images to digital RGB true colour aerial images, and finally to the digital colour infrared (CIR) sensor data used
- 55 today. In addition to the application of stereo-image-based analysis on various sample grids, comprehensive datasets have been
- developed and produced.
- 57 The use of historical aerial images for 3D forest reconstruction is limited, with most studies focused on 2D changes in tree and
- 58 canopy cover at local scales using orthoimages (e.g., Kadmon and Harari-Kremer, 1999; Morgan and Gergel, 2010; Kulha et
- al., 2018) and texture analysis (Hudak and Wessman, 1998; Kupidura et al., 2019). In Central Switzerland, Waser et al. (2008a,
- 60 b) used scanned colour infrared aerial images to generate DSMs and quantify tree/shrub cover changes between 1997 and
- 61 2002. Recent research has focused on methods based on artificial intelligence (AI) to extract information on woody vegetation
- along alpine treeline ecotones, tree cover (Wang et al., 2022), and forest cover (Hufkens et al., 2020) from historical aerial

DSM time series from historical aerial images. As changes in the height of forest canopies over time represent a key aspect of forest dynamics, further studies have been conducted to explore the use of historical images for tracking long-term changes in canopy height (Nurminen et al., 2015; Bożek et al., 2019; Hufkens et al., 2020) and forest stand age (Vastaranta et al., 2015) and for describing the evolution of forest successional stages in tropical forests (Berveglieri et al., 2016, 2018). Here, we present a highly automated approach to process scanned aerial images (hereafter referred to as 'historical aerial images') for generating countrywide DSMs and VHMs in Switzerland. Expanding on the work by Heisig and Simmen (2021). who generated a single countrywide orthoimage of Switzerland from images taken between 1985 and 1991, we processed all scanned images available from swisstopo, the Swiss Federal Office of Topography (swisstopo, 2024a), acquired over Switzerland between 1979 and 2006, Countrywide coverage was obtained using image acquisition intervals of approximately seven years, leading to four countrywide DSM products for the epochs 1979–1985, 1985–1991, 1991–1998, and 1998–2006. To derive VHMs, we normalised the elevation values from the historical DSMs by subtracting the available countrywide digital terrain model (DTM; swissALTI3D version 2017, swisstopo). We assessed the quality of the generated DSMs by evaluating the completeness of the image-matching process across different land cover types and the vertical accuracy of the historical DSMs by comparing elevation values with: (i) the reference DTM on sealed surface points, (ii) geodetic elevation points on a national scale, and (iii) manual stereoscopic elevation measurements from six representative study sites in Switzerland. We close the article by highlighting the potential applications of these datasets in research on forest dynamics and management.

orthoimages. The study by Véga and St-Onge (2008) was among the first where forest canopy growth was quantified using

#### 2 Dataset and methods

63

64

65

66

67

68

69

70

71

72

73

74

75

76

77

78

79

80

81

82

83

84

8586

87

88

89

90

91

92

93

#### 2.1 Historical aerial stereo imagery of Switzerland and study sites selection

DSMs and VHMs were generated from approximately 32'000 historical images acquired with an RC10 panchromatic aerial camera manufactured by Wild Heerbrugg (currently owned by Leica Geosystems, Heerbrugg, Switzerland). Multiple airborne campaigns were conducted from 1979 to 2006 covering the entire 41,285 km² of Switzerland, with an elevation range between 197 and 4634 m a.s.l. Figure 1 shows the image footprints of the stereo pairs used to generate the DSMs, along with the corresponding year of acquisition and the total number of images per epoch. Each campaign spans approximately 7 years to cover the entire country. Image acquisition was guided by the 1:25000 map sheet units (12 x 17.5 km) representing the topographic maps of Switzerland (swisstopo, 2024b). The first countrywide coverage was obtained from the acquisition campaign that took place between 1979 and 1985 (epoch 1), followed by subsequent campaigns from 1985 to 1991 (epoch 2), 1991 to 1998 (epoch 3), and 1998 to 2006 (epoch 4) (Fig. 1).

The primary purpose of these photograph acquisitions was to update the topographic maps produced by swisstopo. The photographs were acquired with approximately 70–80% front overlap and 30–40% side overlap. The average flight height for

94 a 95 s 96 o 97 a 98 a 9

all datasets was approximately 4,000 m above the ground, with an image scale of about 1:25,000. The photographs were scanned with a resolution of 14 µm using a Leica DSW700 scanner (swisstopo). This resulted in an average ground sample distance (GSD) of around 0.35 m in the scanned images, with larger variations in high-elevation areas. Historical aerial images are freely available on swisstopo's website (swisstopo, 2024a) and are provided with exterior orientation parameters, as well as camera calibration protocols containing interior orientation parameters such as focal length and fiducial mark values.

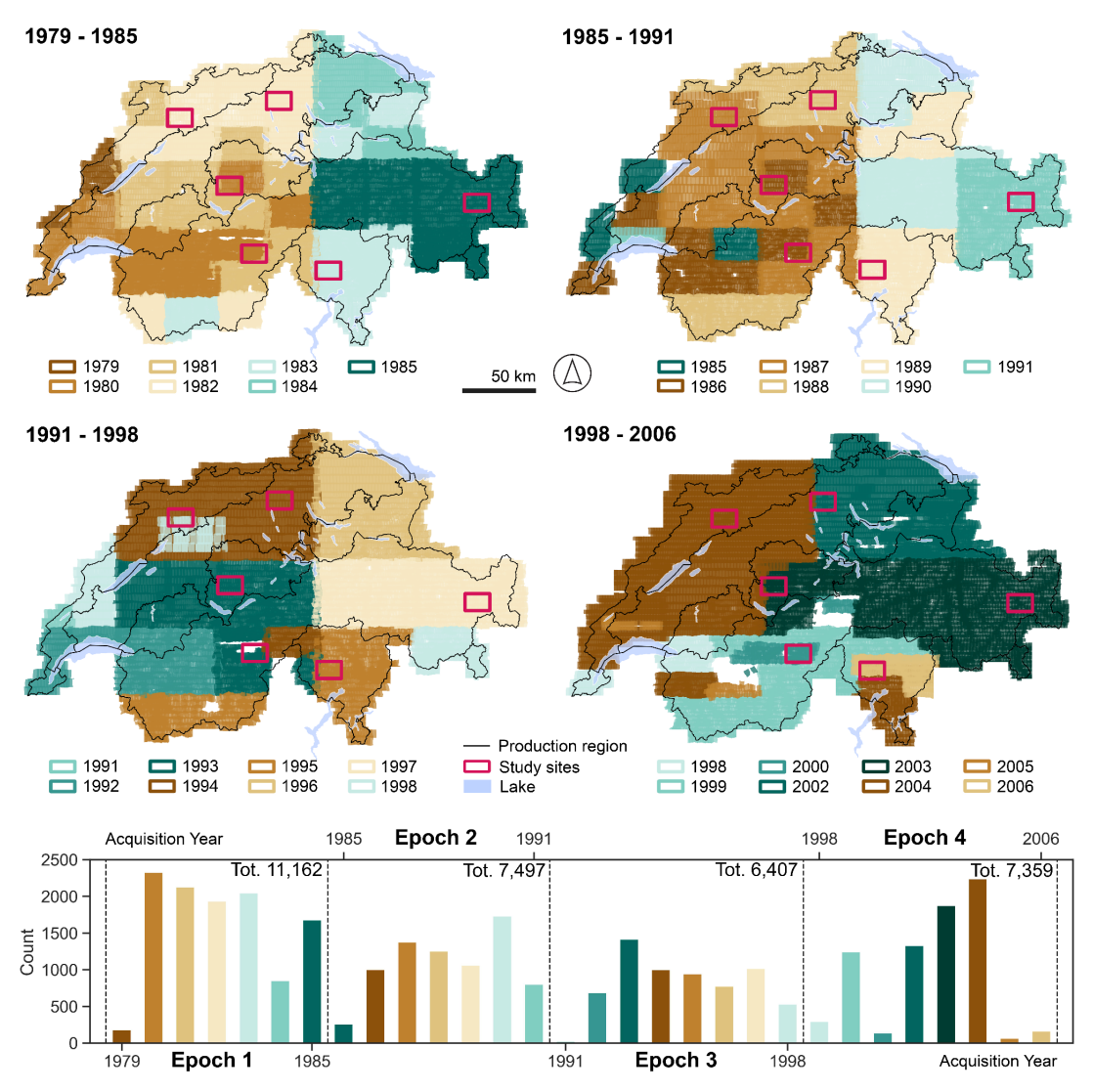


Figure 1: Stereo footprint coverage over Switzerland for the four epochs and the number of images used for the respective digital surface model (DSM) generation (barplot, bottom). There is an overlap of acquisition years between adjacent epochs, but images from the same year cover different forest production regions in each epoch.

In the Swiss NFI, Switzerland is characterised by different types of landscapes and is divided into five main forest production regions: the Jura in the northwest (1), the Swiss Plateau (2), the Prealps (3) between the Swiss Plateau and the Alps, the Alps

(4/4a), and the Southern Alps (5) (Fig. 2). These regions exhibit different climatic and topographic characteristics, such as land cover classes, elevation ranges, tree species and forest structures (Tab. 1). Six representative study sites of approximately 210 km<sup>2</sup> each (i.e., one map sheet) were selected within these regions (Fig. 2). In the Alps region, an additional study site encompassing the tongue of the Grosser Aletsch Glacier was included.

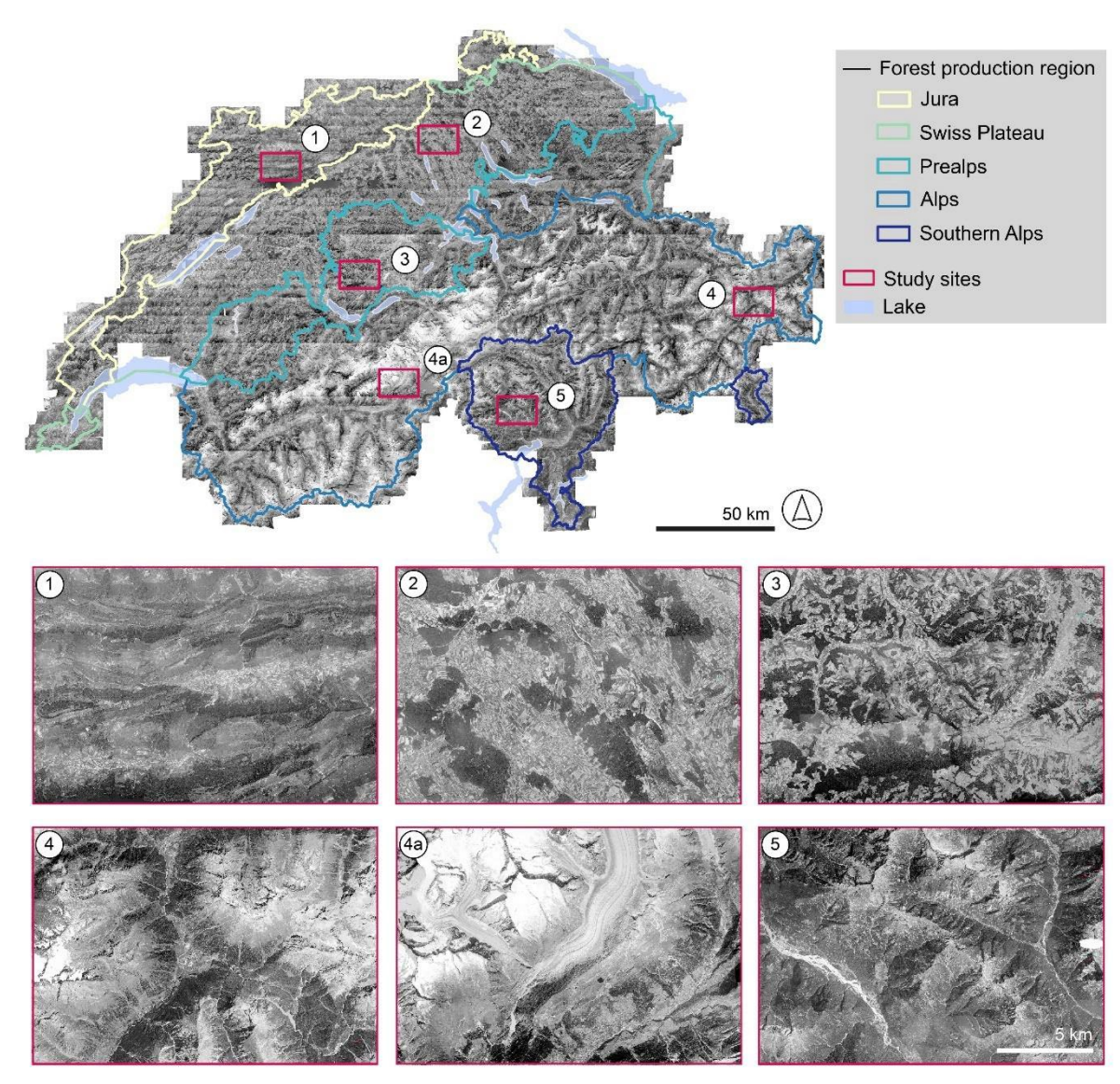


Figure 2: The Swiss NFI forest production regions (1 = Jura, 2 = Swiss Plateau, 3 = Pre-Alps, 4 = Alps, 5 = Southern Alps) in Switzerland and the respective location of the study site for each region, along with the generated orthoimage for epoch 1 (1979–1985). An additional study site (4a) was selected for the Alps forest production region.

Table 2: Forest production region characteristics. Topographic parameters are based on the swissALTI3D digital terrain model (DTM) version 2017. Forest parameters are based on the Swiss National Forest Inventory (NFI).

Forest production region		Area	Elevation range	Mean slope	Forest cover	Forest type					
No.	Name	(km²)	(m a.s.l.)	(°)	(%)	pure coniferous (%)	mixed coniferous (%)	mixed deciduous (%)	pure deciduous (%)		
1	Jura	4935.4	244-1677	12.3	39.5	28.6	25.5	18.8	22.3		
2	Swiss Plateau	9412.8	311–1685	7.2	24.2	37.8	22.9	13.6	22.1		
3	Prealps	6608.1	370-2899	19.8	32.5	53.7	22.4	8.2	9.6		
4 5	Alps Southern Alps	16782.6 3545.7	370–4634 192–3899	28.9 31.6	21.0 39.2	71.0 31.7	9.6 7.4	5.8 5.2	8.6 51.9		

#### 2.2 DSM and VHM generation

114

115

116

117

118

119

120

121

122

123

124

125

126

127

128

129

130

131

132

133

134

135

136

137

The scanned input images, auxiliary data, and the steps used to generate the DSMs and the VHMs are illustrated in Fig. 3. The countrywide DSMs and VHMs are provided at 1 m spatial resolution in the Swiss projected coordinate system CH1903+ / LV95 (EPSG code 2056), and height information is supplied in LN02 (EPSG code 5728) where applicable.

The scanned historical images were processed using the commercial photogrammetric software SocetSet (v5.6.0) by BAE Systems (Falls Church, USA). With known interior and exterior orientation parameters, the historical images were imported to the software through the "frame import dialogue". The import process was separately done for all images originating from the same camera. During the frame import process, camera calibration values were entered, and fiducial marks were primarily detected using automatic fiducial detection, implemented in the frame import workflow. Where this automatic approach failed, manual measurement of fiducial marks was conducted. Subsequently, the DSMs can be generated using the Next-Generation Automatic Terrain Extraction (NGATE) package implemented in SocetSet (DeVenecia et al., 2007). The exterior orientation information for the images from epochs 1, 2 and 4 was derived by swisstopo within the framework of the Swiss Land Use/Cover Statistics program around 2004. This image orientation was performed using ground control points (GCPs), visible in the historical imagery, and in more recent already-oriented digital stereo images available from swisstopo. The elevation of the GCPs was stereoscopically extracted from the digital images. This image orientation resulted in accurate horizontal positioning but biases in the Z direction, ranging from 1 to 5 m, randomly distributed across Switzerland. Therefore, the DSMs from these epochs were vertically corrected, as described in section 2.2.2. In contrast, the images for epoch 2 were recently oriented using a highly automated workflow, as described by Heisig and Simmen (2021). Their study reported planimetric residuals of the GCPs for the different triangulation blocks, which ranged from 2 to 3 pixels (0.6-0.9 m RMSE). Additionally, a comparison between the derived historical orthomosaic and a reference orthomosaic at sample points evenly distributed over Switzerland revealed a median difference of 1 m, with no systematic bias across Switzerland (Heisig and Simmen, 2021).

Although there are no documented values for the planimetric accuracies for the images from epochs 1, 3 and 4, comparisons of the ortho mosaics from those epochs to one derived from epoch 2 show similar results.

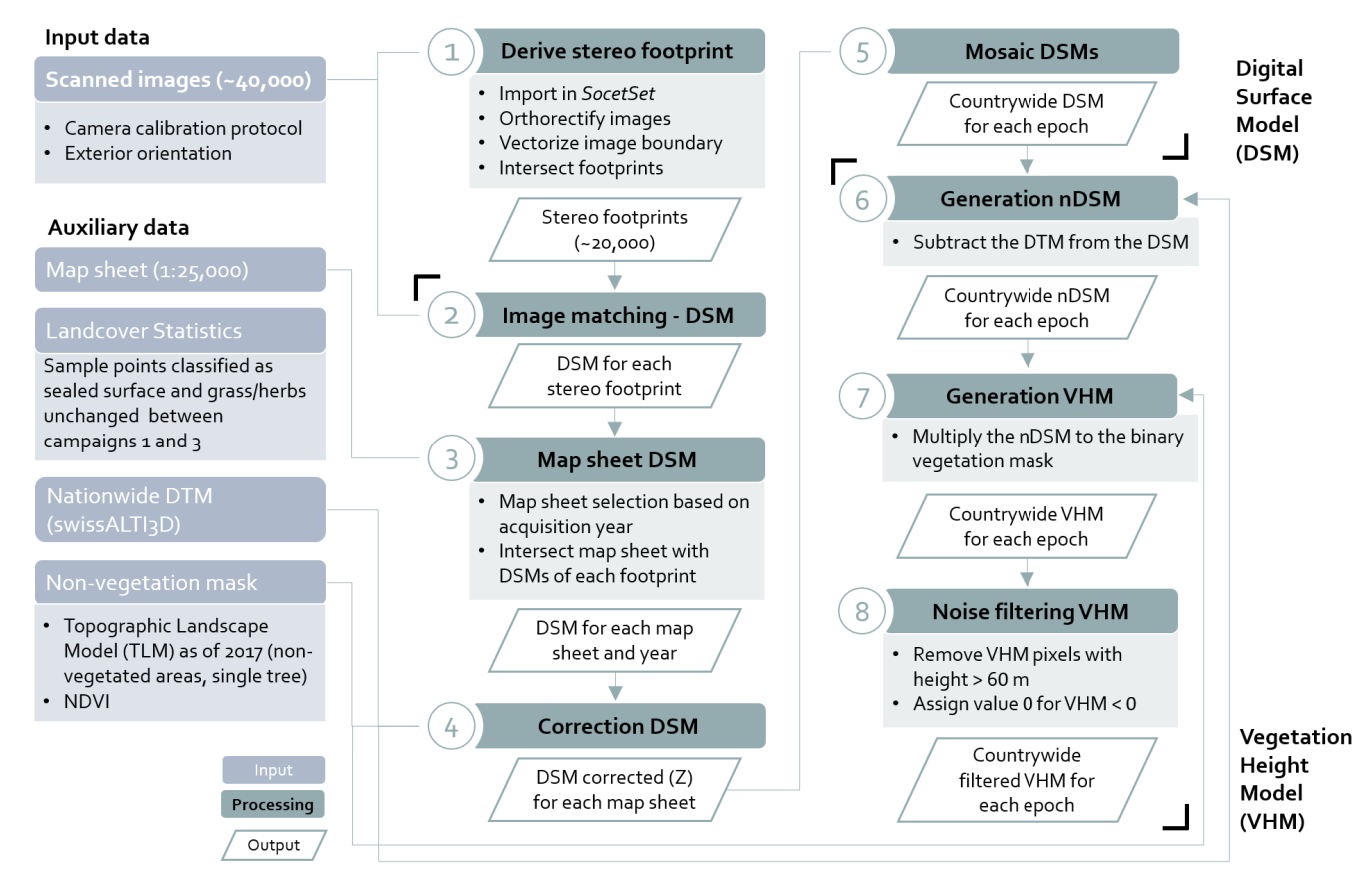


Figure 3: Workflow of historical image processing and countrywide digital surface model (DSM) and vegetation height model (VHM) generation.

#### 2.2.1 Image-matching and DSMs

The DSM generation process using the NGATE package followed a highly automated workflow. To handle the DSM reconstruction process, image-matching was performed on distributed machines for single stereo footprints (i.e., stereo pairs). In the initial step, the footprint for each image was calculated, and the footprints of adjacent images along the same flight line (belonging to the same acquisition year) were intersected to create stereo footprints. In total, 20,346 stereo footprints were processed. All stereo footprints were stored in a table on a PostGIS database, which was used to control the image-matching process running on distributed virtual machines. Since stereo pairs were formed only from the neighbouring images along the same flight line, multi-image-matching was not involved in this process.

NGATE provides several predefined correlation/matching strategies for different types of image content, such as urban, flat and low-contrast areas. To ensure the extraction of accurate and complete elevation information across different land cover

types, two strategies were adopted, namely urban and low contrast. The urban strategy utilises internal correlation parameters that account for strong elevation discontinuities, which represents the most prominent characteristics of forest canopies. In contrast, the low-contrast strategy aims to identify congruent points on highly homogeneous surfaces, such as meadows or bare land. While image-matching in NGATE is conducted on every pixel of the input imagery, the resulting output file represents a regular grid of three-dimensional (XYZ) coordinates. Optionally, this grid can include information about successful image-matching or interpolation for the given pixel, as indicated by the Figure of Merit value, a product derived by the software. The spatial resolution of the output DSM is user-defined and, in our case, was set to 1 m, approximately three times the GSD of the scanned images.

The image-matching using the two strategies resulted in two separate DSMs for each stereo footprint. These two DSMs were combined into one DSM by including all successfully matched points from the urban strategy and filling remaining gaps with correlated points from the low-contrast strategy, where available.

#### 2.2.2 DSM merging and vertical correction

- The 20,346 DSMs resulting from image-matching of the single stereo footprints were merged to the level of the 1:25,000 map sheets, which were already used to guide the image acquisition campaigns (see section 2.1). For each map sheet geometry, all DSMs from the same epoch that corresponded to individual stereo footprints were selected based on spatial intersection. They were then merged and cropped to fit the extent of the map sheet, which typically included around 50 stereo footprints in flat areas and up to 150 in high-alpine regions. Since adjacent stereo footprints spatially overlapped, the pixels in these overlapping areas often included multiple elevation values. To address this, the elevation values were merged using the median height. Grid cells without any successfully matched elevation information were interpolated using a triangular irregular network (TIN) surface.
- The exterior orientation of the images from epochs 1, 3 and 4 resulted in a vertical offset of up to 5 m between the DSMs and the reference DTM on stable terrain (i.e., sealed surfaces and grass/herb points; see section 2.3.1). Therefore, the DSMs from these epochs were vertically corrected. For consistency, this correction was also applied to the DSM from epoch 2, resulting in neglectable changes due to the already precise horizontal and vertical orientation.
- 177 The vertical correction was performed on the merged map sheet DSMs as illustrated in Fig. 4.
- The workflow consisted of calculating the difference between the reference DTM (swissALTI3D version 2017; see section 2.2.3) and the generated DSM at points corresponding to the classes 'sealed surface' and 'grass/herb' in the first and third campaigns of the Swiss Land Use/Cover Statistics program (1979–1985 and 2004–2009, respectively; see section 2.3.1). With this approach, only points with an unchanged land cover classification were used. Outliers were filtered out based on mean  $\pm$ 1 standard deviation (Std), calculated within a moving window of 50 × 50 pixels. The median of the remaining elevation differences was then calculated for each of the 1,200 regular grid cells per map sheet. The number of regular grid cells was determined through an empirical approach, ensuring that each grid cell contained enough difference values to yield a valid median and that there were sufficient grid cells per map sheet to enable the interpolation of a continuous correction surface

using spline interpolation. This correction surface was subsequently applied to the resulting DSMs at the map sheet unit level to correct elevation bias.

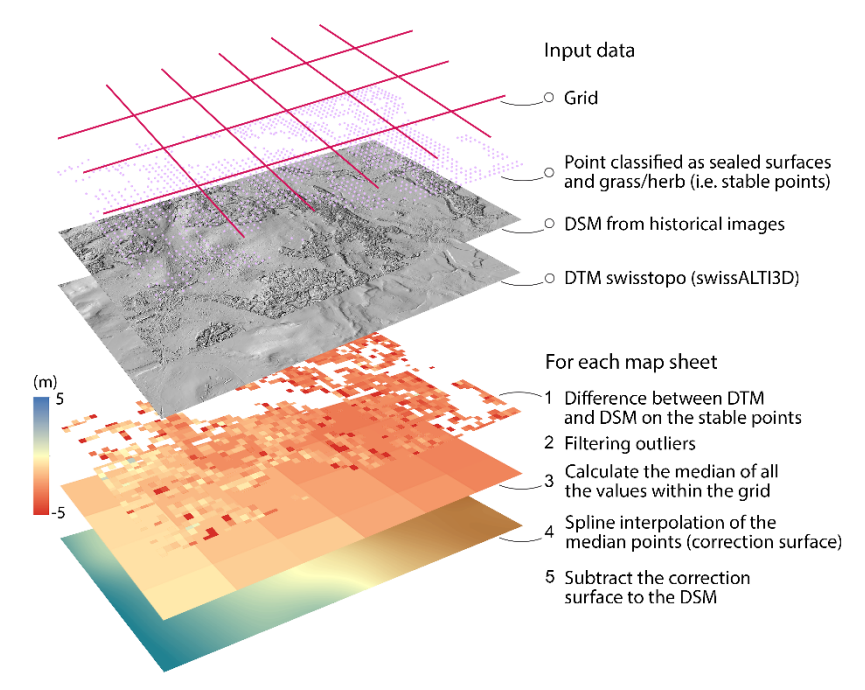


Figure 4: Illustration of the workflow to correct the elevation bias in the historical digital surface models (DSMs) for each map sheet. The correction is based on the elevation difference between the reference digital terrain model (DTM) and the historical DSM for sample points classified as sealed surfaces and grass/herb.

#### 2.2.3 Countrywide DSMs and VHMs

After correcting for randomly distributed elevation biases in each map sheet DSM and epoch (as described in section 2.2.2), all the corrected map sheet DSMs from the same epoch were mosaiced to a single DSM as a Geotiff file, covering the whole of Switzerland.

The four countrywide VHMs were derived by calculating the difference between the historical DSMs and the reference DTM (swissALTI3D version 2017, swisstopo; see workflow in Fig. 3). This process resulted in a normalised DSM (nDSM), representing the heights of all objects above ground. Note that the reference DTM was resampled from the default resolution of 2 m to 1 m to match the resolution of the generated DSMs. The swissALTI3D DTM is based on airborne laser scanning data for elevations up to 2000 m a.s.l., with an overall point density of 0.5 points/ $m^2$  and a vertical accuracy of  $\pm 0.5$  m (standard deviation). Above 2000 m a.s.l., elevation information is derived by image-matching and manual editing, yielding a documented vertical accuracy of 1–3 m on average (swisstopo, 2024c).

nDSM raster cells with values > 60 m were considered outliers due to erroneous image-matching and thus were replaced by 'no data'. Next, the VHM (i.e., the nDSM of vegetated areas) was generated by assigning a height above ground of 0 m to all non-vegetated objects. To achieve this, a binary non-vegetation mask (0 = non-vegetation and 1 = vegetation) was created by

combining information from the topographic landscape model (TLM; swisstopo, 2024d) and a normalised difference vegetation index (NDVI) map obtained from aerial orthoimages of the years 2009–2015. All areas classified in the TLM as building, street, and water surface, as well as pixels with an NDVI < 0.1, were set to 0. To retain vegetation close to buildings and streets in the VHMs, single trees and hedges from the TLM were buffered by 15 m and set to 1. This non-vegetation mask was multiplied by the nDSMs. The resulting VHMs have a spatial resolution of 1 m, consistent with the historical DSMs.

#### 2.3 Quality assessment of the DSMs

- The quality of the generated DSMs was assessed by analysing: (1) the completeness achieved through the image-matching
- 213 process over different land cover types and (2) the elevation accuracy based on elevation differences to reference datasets (see
- section 2.3.1). The elevation differences were calculated consistently as the historical DSMs minus the reference data.
- Therefore, positive differences indicate that historical DSMs had positive biases, i.e., that the reference data was lower than
- the historical DSM. Quality assessment was performed and reported for the six selected areas and the countrywide DSMs.

#### 2.3.1 Reference data

206

207

208

209

210

211

- The reference dataset used to assess the completeness of the image-matching process over different land cover classes consisted
- of sample point interpretation on a regular 100 m grid across Switzerland. These sample points were collected by the Swiss
- 220 Federal Statistical Office in the framework of the Swiss Land Cover/Use Statistics program (BFS, 2024) (Fig. A1). These
- countrywide land cover statistics campaigns took place in 1979–1985, 1992–1997, 2004–2009 and 2013–2018. The
- completeness for epoch 1 was assessed, and the reference data from the 1979–1985 campaign was used. This dataset comprised
- 223 121,896 points for the 6 selected areas. The 27 specific land cover classes were grouped into 6 categories; (1) sealed surface,
- 224 (2) bare land, (3) grass/herb, (4) shrub, (5) closed forest, and (6) glacial and perpetual snow.
- The vertical accuracy of the DSMs was assessed by comparing the elevation with three reference datasets (i.e., DSM minus
- reference data). First, the sealed surface points that remained unchanged between the 1979–1985 and 2004–2009 campaigns
- 227 were used. At these points, the elevation differences between the DSMs and the reference DTM were calculated. The reference
- DTM was the same as the one used for generating the VHM (see section 2.2.3).
- 229 The second reference dataset comprised 565 selected geodetic control points (i.e., measured with GNSS or triangulation)
- distributed throughout Switzerland. This dataset is monitored and maintained by swisstopo; the documented vertical accuracy
- ranges from 0.003 to 0.1 m, with 42% of the points showing accuracies of 0.05 m or better. For the remaining ones, an accuracy
- of 0.1 m is documented (swisstopo, 2023). These geodetic points enabled a completely independent estimation of the vertical
- accuracy of the derived DSMs.
- As a third reference dataset, 16,650 stereoscopic elevation measurements conducted by a stereo-image interpreter at the Swiss
- 235 Federal Institute for Forest, Snow and Landscape Research (WSL) were used. The data collection scheme was the same as in
- the NFI (Ginzler, 2019). These measurements were derived only for epoch 1 and within the 666 forest plots of  $50 \times 50$  m area
- 237 intersecting the 6 study sites (Fig. 1). For each forest plot, 25 elevation measurements were extracted on one of the overlapping

stereo pairs used to create the historical DSM (Fig. A1). In addition, the six land cover classes used to assess completeness were assigned to each stereo measurement. The 'closed forest' land cover class was further divided into coniferous or deciduous trees. It is worth noting that this reference data was used to evaluate agreement rather than serving as a measure of accuracy, since the stereoscopic measurements have some inherent inaccuracies and the measurement was done on one stereo pair only.

## 2.3.2 DSM completeness

Completeness is an essential quality measure for photogrammetric DSM generation. Here, it was computed as the percentage of successfully matched points out of the potential total number of matched points within a defined spatial unit. Completeness was calculated within circles with a radius of 5 m centred around points of the land cover statistics dataset. Then, the mean completeness was calculated for the six land cover classes (i.e., sealed surface, bare land, grass/herb, shrub, closed forest, and glacial and perpetual snow). Completeness values were calculated for all four epochs from the DSMs of the six study sites before cropping to the actual map sheet extent (see section 2.2.2).

Vertical accuracy was calculated as the difference between the DSMs and the reference dataset (see section 2.3.1). First, the

elevation differences between the DSMs and the reference DTM were calculated at points classified as sealed surfaces. Sealed

#### 2.3.3 Vertical accuracy

surface points closer than 10 m to historical and current houses and the forest boundary were removed. In addition, points classified as grass/herb and bare land were used to quantify the elevation bias of the DSMs to terrain slope, aspect and elevation. Sealed surface points were not used in this investigation because they were mainly located in flat areas. In a second analysis, the elevation values of the DSMs were compared with approximately 500 independent geodetic points. Finally, > 16,000 stereoscopic elevation measurements were used to assess the performance of the image-matching workflow on deciduous and coniferous trees, the primary target objects.

To calculate the statistical measures, differences greater than ±50 m between the DSMs and the reference measurements were excluded because such values indicated a failure in image-matching due to cloud cover or saturated images, yielding unrealistic elevation values. From the remaining differences, robust statistics, such as the median and the normalised median absolute deviation (NMAD) were calculated, as biases in spatial datasets are often not normally distributed (Höhle and Höhle, 2009). The NMAD is defined as 1.4826\*MAD (median absolute deviation). Root mean square error (RMSE) values were additionally calculated, as a standard quality metric to facilitate the comparison of our results with those from other studies. RMSE values were determined after applying a robust outlier removal (median ± 5 NMAD).

#### 3 Results

#### 3.1 Generation of DSMs

Four countrywide DSMs were generated successfully with the NGATE package of SocetSet. Data voids are related to the lack of stereo images (Fig. 2) or to unsuccessful image-matching in saturated or cloudy areas. Figure 5 shows the hillshaded DSM for the epoch 1979–1985 for the six study sites.

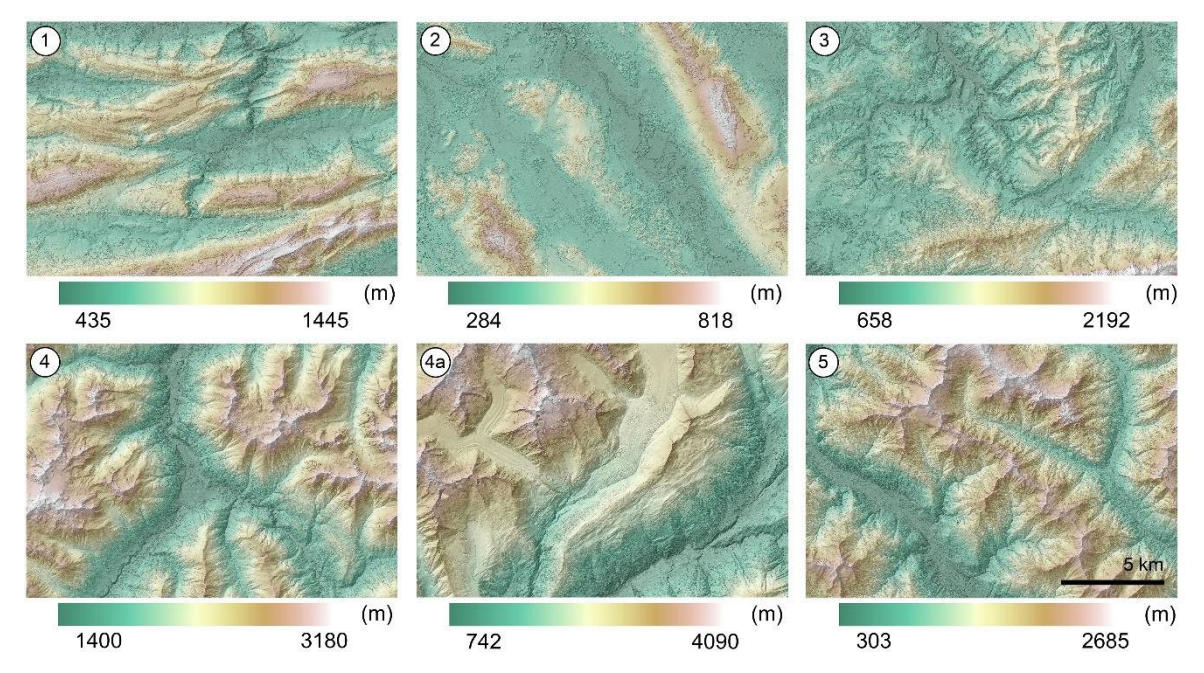


Figure 5: Hillshaded digital surface models (DSMs) for the six selected study sites and epoch 1 (1979–1985). The year of the DSM is 1982 for sites 1 and 2, 1980 for site 3, 1985 for sites 4 and 4a, and 1983 for site 5.

## 3.2 DSM completeness

Figure 6 shows the DSM completeness percentages for epoch 1 and the six land cover classes: sealed surface, bare land, grass/herb, shrub, closed forest, and glacial and perpetual snow. The number of sample points for each class is also provided in the figure. Completeness results for epochs 2, 3 and 4 are provided in Appendix A (Fig. A2), and Table A1 shows the corresponding mean values. The lowest completeness occurred in areas classified as glacial and perpetual snow, with a mean completeness of 65% across the four epochs. This result was expected, due to the texture less black-and-white images of these surfaces, which resulted in poor image-matching performance. The highest completeness was achieved for sealed surfaces, with a mean of 98%. For the classes bare land, shrub and closed forest, the mean completeness was approximately 90%, whereas the grass/herb class had a mean of 79%. However, the completeness for the grass/herb class was higher for epochs 2, 3 and 4 (Fig. A2), with a minimum value of 84%.

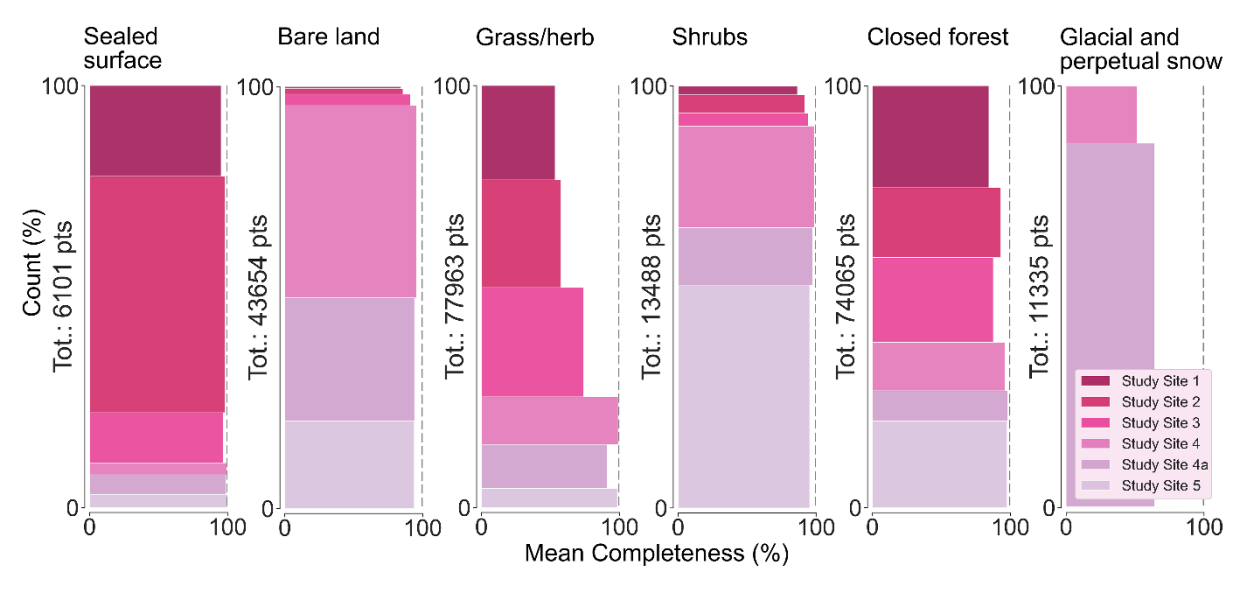


Figure 6: Distribution of the mean completeness values (as percentages) for epoch 1 across the six study sites and the six land cover classes – sealed surface, bare land, grass/herb, shrub, closed forest, and glacial and perpetual snow. The snow class is only present in study sites 4, 4a and 5. Note that for some classes and study sites, the number of points is minimal. For example, there are only 18 points in study site 5, which is equivalent to 0.15% for the class 'glacial and perpetual snow', and therefore the horizontal bar is not visible.

#### 3.3 DSM vertical accuracy assessment

The vertical accuracy of the DSMs for each epoch was assessed by comparing them with three reference elevation datasets (see section 2.3.1). Figure 7a shows the spatial distributions of the sealed surface points and the reference geodetic points, while Table 2 summarises the statistical measures. Sealed surface points exhibit a clustered distribution in low-elevation areas (i.e., regions 1, 2 and 3) and a sparser distribution in the Alps and Southern Alps (regions 4 and 5, respectively). No clear systematic difference is observed when visualising the positive and negative elevation differences at sealed surface points between the DSM from the first epoch and the DTM. However, plotting the frequency distribution of elevation differences across the entire country reveals a positively skewed distribution for all epochs (Fig. 7b). Points on the sealed surface that were suboptimally located, such as those near urban areas and the forest edge, were removed. However, several values still exceed 10 m. The positive skew is also reflected in the median values of the elevation differences (Table 2), with values between 0.08 and 0.16 m and a maximum NMAD of 0.86 m.

In the analysis of the vertical accuracy of the DSMs in comparison to independent geodetic points, the median is around zero, with an NMAD of < 1 m (Table 2). Note that the number of geodetic points is two orders of magnitude smaller than the sealed surface points and more evenly distributed over the country. Additionally, the number of geodetic points varies slightly across the different epochs due to the spatial coverage of the image-matching results (e.g., cloud cover and image saturation). The differences between the DSMs and geodetic points have a more symmetric distribution for all four epochs, with few positive differences > 10 m (Fig. 7c).

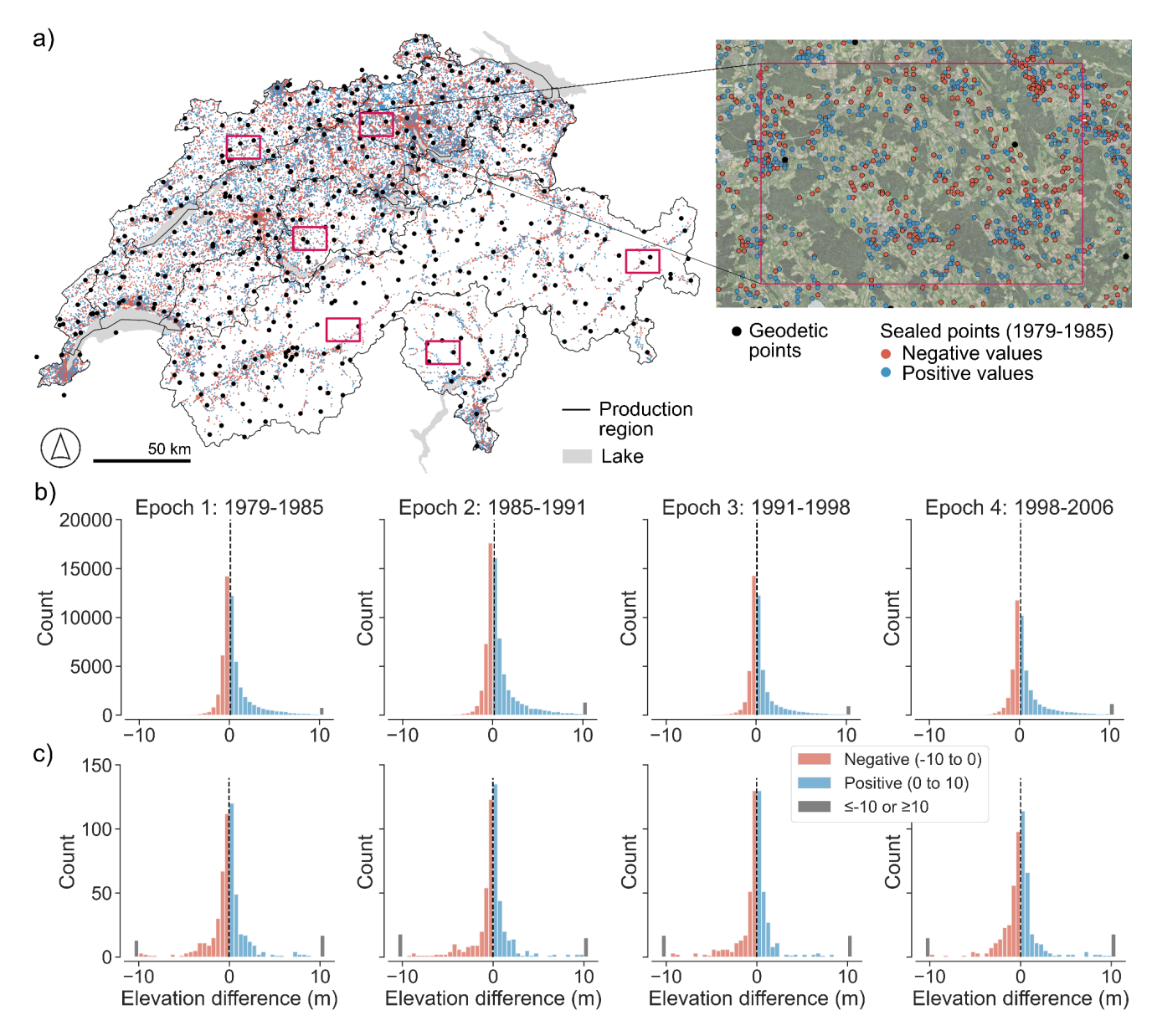


Figure 7: (a) Spatial distribution of the sealed surface points and the geodetic points used for the vertical accuracy assessment of the historical digital surface models (DSMs). Sealed surface points are depicted in blue and red, representing the positive and negative differences, respectively, between the DSM for epoch 1 and the reference digital terrain model (DTM, swissALTI3D). The inset shows the distribution of the sealed surface points and the geodetic points for study site 2, overlaid on the orthophoto for the year 2021 (swisstopo, 2023). Frequency distributions of the elevation difference in metres between the DSM and the DTM (b) on sealed surface points and (c) between the DSM and the geodetic points for the whole of Switzerland for the four epochs. The vertical dashed line indicates the median value. The bin size is 0.5 m. The histogram shows the distribution before the filtering used for the root mean square error (RMSE) calculation.

Table 2: Elevation difference between the historical digital surface models (DSMs) and the digital terrain model (DTM) over the sealed surface points and the geodetic points over Switzerland for the four epochs. The number of points before and after outlier filtering is reported; the latter number was used for the root mean square error (RMSE) calculation.

Epochs	A	Accuracy	on sealed	surface points		Accuracy on geodetic points					
	No. points (±50 m)	Median (m)	NMAD (m)	No. points after filter (± 5 NMAD)	RMSE (m)	No. points (±50 m)	Median (m)	NMAD (m)	No. points after filtering (± 5 NMAD)	RMSE (m)	
Epoch 1	54901	0.10	0.81	50663	1.14	551	-0.05	0.96	498	1.35	
Epoch 2	71685	0.16	0.86	66140	1.20	542	-0.03	0.82	471	1.17	
Epoch 3	49275	0.08	0.68	44671	0.95	536	-0.02	0.78	468	1.05	
Epoch 4	46451	0.13	0.85	42499	1.19	525	-0.00	0.98	470	1.27	

The elevation difference between the historical DSMs and the DTM over grass/herb and bare land points shows no significant bias with slope, aspect or elevation, as shown in Figure 8. However, for elevations above 3000 m a.s.l. and slopes greater than  $45^{\circ}$ , the NMAD increases drastically, exceeding 2 m for all four countrywide DSMs. However, points within these intervals represent only approximately 5% (slope) and 1% (elevation), as shown in the histograms in Fig. 8. The elevation bias dependence on aspect shows a potential shift, with median values below 0.5 m and a constant NMAD of  $\pm$  0.8 m for all datasets and aspect intervals.

The agreement between the stereoscopic measurement (see section 2.3.3) taken within the NFI plots and the historical DSM of epoch 1 is reported in Table 3 for the different land cover classes, including a division of the closed forest class into deciduous and coniferous trees. Figure 9 shows one NFI plot with the stereo measurement location and elevation values compared with the DSM profile. As shown in Table 3, the closest agreement is observed for the sealed surface class, with a median difference of -0.19 m and an NMAD of 0.63 m, comparable to the results obtained when analysing the difference between the DSM and DTM for this land cover class (see Table 2). For the grass/herb class, the differences to the stereo measurements exhibit a similar offset but with a larger spread, with a median of 0.15 m and a NMAD of about 1 m. Sample points from the shrub and bare land classes show a wider spread, with NMAD values of 1.62 m and 1 m, respectively, and larger systematic biases, with median values greater than 0.4 m. The weakest agreement is found for the closed forest class, where deciduous and coniferous trees yield comparable results, with median values of about 1.8 m and NMAD values of up to 3.77 m.

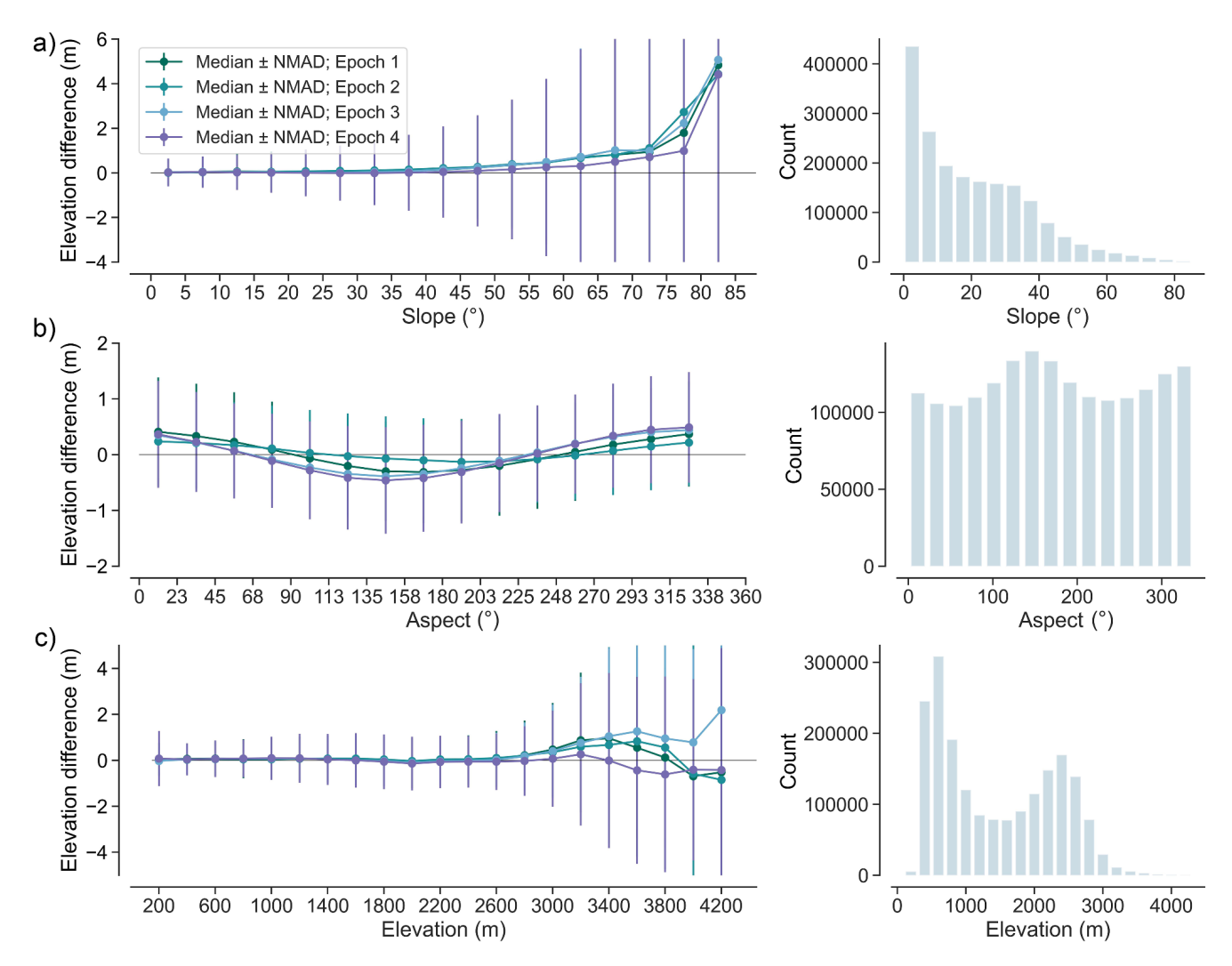


Figure 8: Elevation differences in grass/herb and bare land points as a function of slope (a), aspect (b), and elevation (c). The histogram on the right shows the number of points for each interval. Elevation differences are calculated as the historical digital surface models (DSMs) minus reference digital terrain model (DTM). Slope, aspect and elevations were derived from the reference DTM.

Land cover class	No. points	Median (m)	NMAD (m)	No. points after	RMSE (m)	
				filtering		
				$(\pm 5 \text{ NMAD})$		
Closed forest, deciduous trees	2917	1.83	2.75	2847	4.25	
Closed forest, coniferous trees	2478	1.77	3.77	2435	5.36	
Grass/herb	6792	0.15	1.02	6508	1.31	
Shrub	424	0.41	1.62	411	2.16	
Sealed surfaces	408	-0.19	0.63	379	0.86	
Bare land	1231	0.74	1.00	1217	1.41	
Glacial and perpetual snow	567	-0.17	2.15	539	2.6	

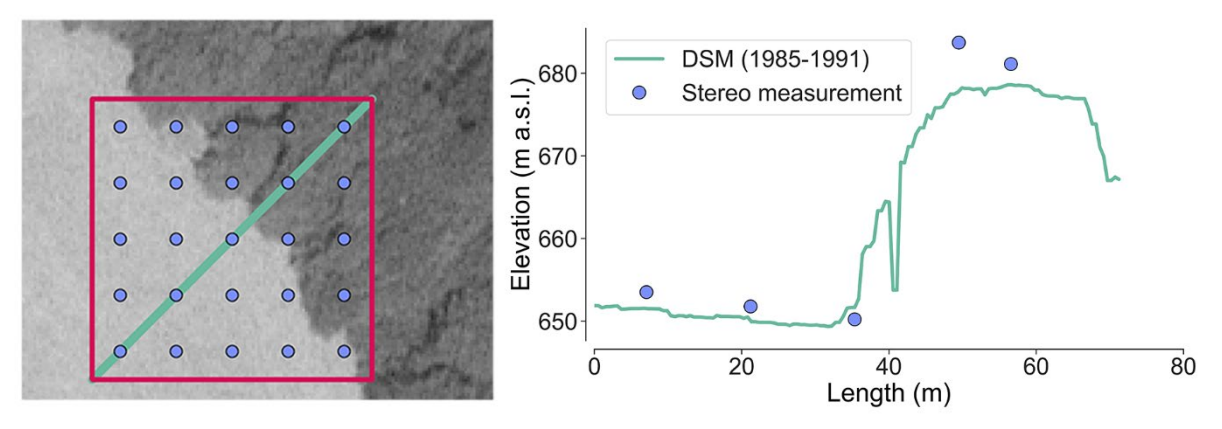


Figure 9: Stereo measurements within a Swiss National Forest Inventory (NFI) forest plot on the historical orthophoto of epoch 1 (left). On the right, a comparison is depicted between the digital surface model (DSM) profile (green line, interval of 1 m) and the elevation values of the stereo measurements.

#### 3.4 VHMs and forest change

Based on the four countrywide historical DSMs for Switzerland, four VHMs were generated by subtracting a countrywide DTM and applying a non-vegetation mask (see section 2.2.3). Figure 10 shows the VHMs and the forest structure for the six study sites for epoch 2. Since the VHMs are direct derivatives of the DSMs, the statement above about the quality remains valid.

Forest dynamics, such as growth, cutting and regrowth between observation epochs are evident over the six study sites, as shown by the height differences of the VHMs between consecutive epochs (Fig. A3). A detailed look at the VHM profiles of study sites 2 and 4 (Fig. 10b) shows minimal change in forest height in mature forest stands (VHM > 20 m), indicating consistency among the VHMs. However, forest growth, cuts or damage followed by regrowth can be detected, for example, between epoch 3 and 4 (cut or damage) and 2022 (regrowth) (Fig. 10b, profile 2, 1250 m - 1500 m). The Swiss Plateau forest production region, where study site 2 is located, was heavily affected by storm damage. Figure 11 shows a small area of the VHM in region 2 for epochs 1, 3 and 4, overlaid by polygons indicating areas damaged by the two largest storm events recorded

in Switzerland: Vivian (25–27 February 1990) and Lothar (26 December 1999). The VHMs effectively capture the stormaffected areas. The VHM of 1982 depicts forest cover in all storm-affected areas, while the 1994 VHM clearly shows the damage caused by storm Vivian. The areas impacted by storm Lothar show mature forest stands in the 1994 VHM, while the heavily damaged areas are visible in the 2002 VHM.

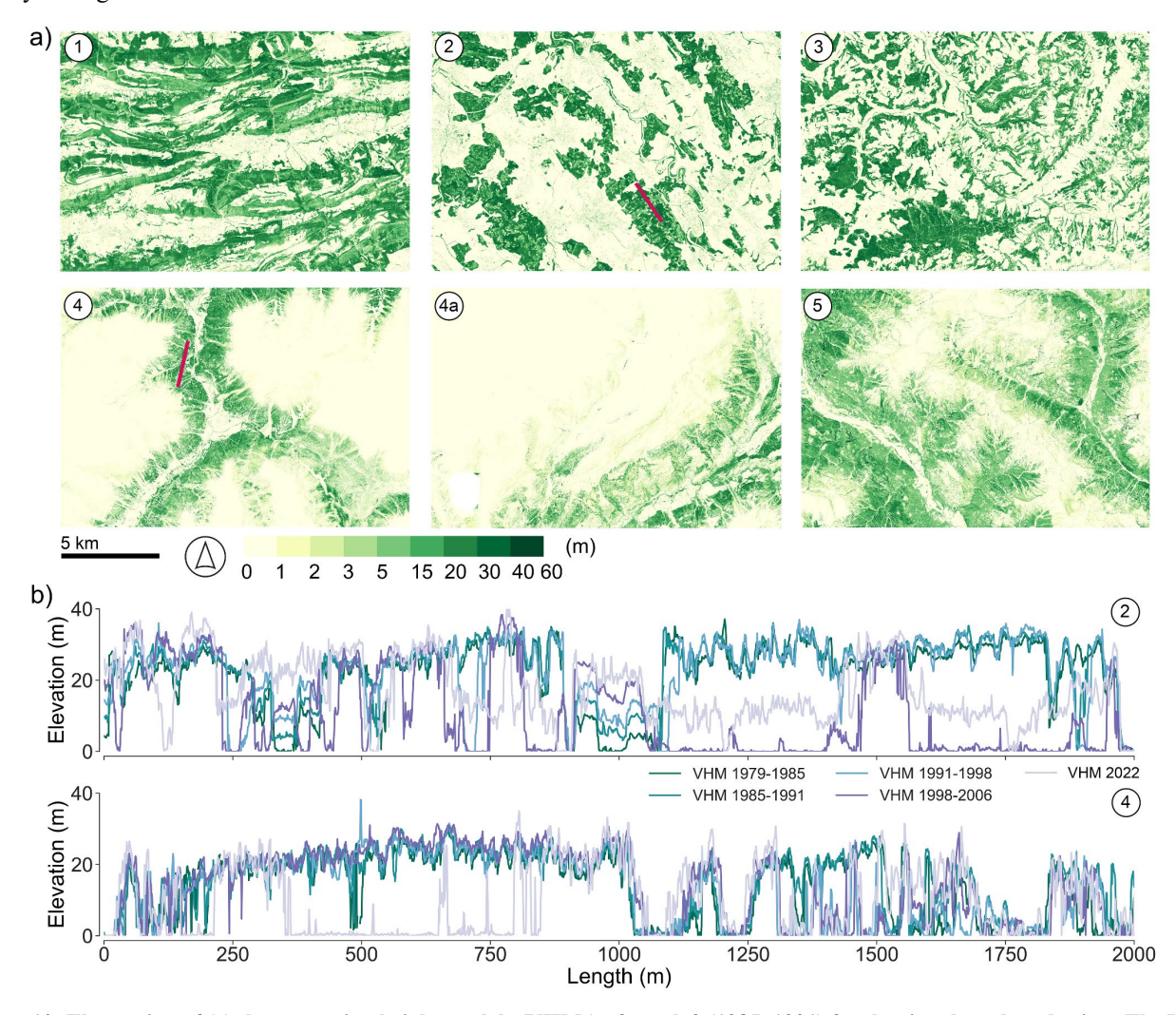


Figure 10: Illustration of (a) the vegetation height models (VHMs) of epoch 2 (1985–1991) for the six selected study sites. The VHMs correspond to the years: 1987 for site 1, 1988 for site 2, 1986 for sites 3 and 4a, 1991 for sites 4, and 1989 for site 5. (b) The profile of the VHMs from historical aerial images for the four epochs and from a modern airborne survey (2022) for study sites 2 and 4. The 2 km profile line is shown in red in (a).

Besides these qualitative results, these historical VHMs have been used in various studies (Price et al., 2020; Ginzler et al., 2021). Ginzler et al. (2021) investigated forest dynamics in Switzerland between 1980 and 2010. Their analysis was based on aggregated average vegetation heights for  $100 \times 100$  m cells derived from the VHMs. They quantified forest dynamics by retrieving the absolute height change over the entire period (sum of absolute differences) and the classified height change

between periods (height gain or loss). The results showed high forest dynamics in the Swiss Plateau and some pre-alpine areas in the northern Alps, while significant parts of the Jura and southern Switzerland showed little change during these 30 years. Price et al. (2020) used the historical VHMs to map and monitor woody above-ground biomass (AGB) dynamics across Switzerland over 35 years (1983–2017). They found a consistent relationship between vegetation height derived from the VHMs and NFI measures of woody AGB across four inventory periods.

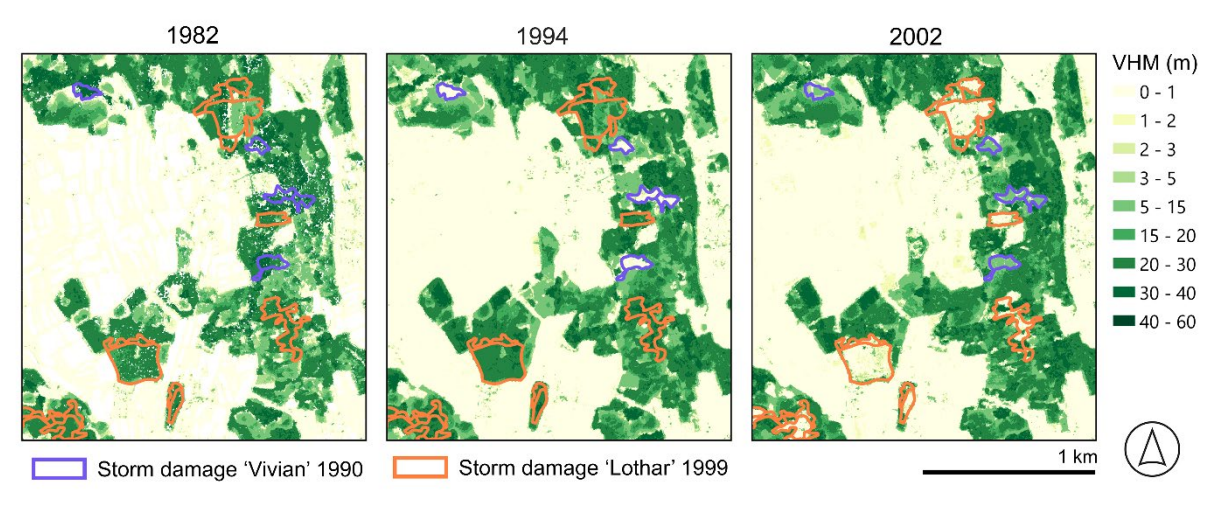


Figure 11: Small extent of region 2 (Swiss Plateau), showing the vegetation height models (VHMs) of epochs 1, 3 and 4, overlaid by polygons indicating areas heavily affected by two major storm events in Switzerland (Vivian: 25 to 27.02.1990 and Lothar: 26.12.1999).

#### 4 Discussion

## 4.1 Potential of countrywide historical DSMs and VHMs of Switzerland

This study underscores the great value of historical aerial images for reconstructing accurate and high-resolution DSMs over approximately three decades. For the epochs 1979–1985, 1985–1991, 1991–1998 and 1998–2006, we successfully processed four countrywide DSMs and VHMs at a resolution of 1 m. The quality of the generated models is sufficient for various geoscience applications, such as the quantification of natural hazards, mass movements, and sediment erosion, and the monitoring of human interference (e.g., deforestation) and urban development. For urban analysis, we recommend using the DSM and normalising it again if needed, as pixel heights larger than 60 m in the VHM were removed. Our historical VHM products show a high level of consistency, suggesting that changes in forest height are real and significant and thus are valuable tools for understanding forest dynamics in Switzerland. This includes the tracking of forest growth and changes in forest cover over time, the differentiation between disturbed (due to management practices or storm events) and undisturbed forests, and the detection of regrowth after disturbance. The clear delineation of storm-damaged areas (e.g., from storms Vivian and Lothar) in our VHM data demonstrates the capability of the models to identify disturbances accurately. By analysing the temporal changes in these areas, we can differentiate between disturbances caused by natural events and those resulting from forest

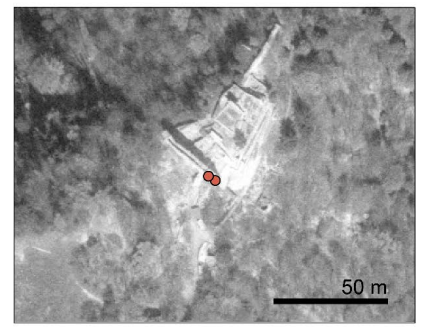
management activities. Therefore, insight can be gained into post-storm regrowth and forest management activities across the forest production regions, and their effectiveness can be quantified, for example in terms of protection forest function. This dataset offers great added value to the Swiss NFI forest management data and supports future management strategies.

#### 4.2 Quality of the DSMs

The completeness of the image-matching across epochs remains nearly constant (Fig. A12). However, an improvement in completeness is observed for grass and herbs, as well as glacial and perennial snow classes, in relation to Epoch 1, although this may vary depending on the study area. In areas with successful image-matching, countrywide accuracy analysis comparing derived DSM elevations to swissALTI3D DTM elevations at sealed surface points shows sub-meter values with a maximum NMAD of 0.86 m. This value is roughly 2.5 times the GSD, although the DSMs were generated at 1 m resolution. A comparison with an independent dataset such as the geodetic points distributed across Switzerland shows comparable accuracy.

The positive bias, where reference data was lower than the historical DSMs, may have resulted from changes in the sealed surface points in urban areas, which could explain the presence of several values more positive than -10 m (Fig. 7b). The comparison with geodetic points also shows outliers with values above 10 m (Fig. 7c), likely related to the suboptimal location of reference geodetic points on objects such as rooftops and statues, which cannot be precisely reconstructed from historical DSM (Fig. 12).





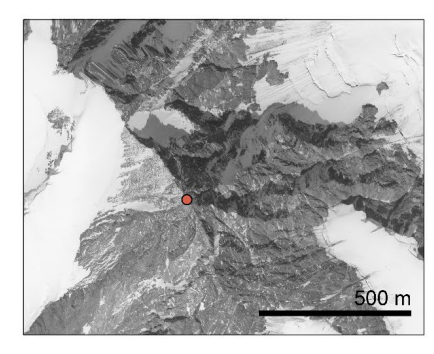


Figure 12: Example of suboptimal locations of geodetic points used for the accuracy assessment. Negative biases over these points are shown in red.

An elevation bias in areas with slopes greater than 45° and elevations above 3000 m a.s.l. (Fig. 8a, c) is present in many photogrammetric products from airborne and satellite sources (e.g., Piermattei et al., 2019) and is more pronounced in historical images with 8-bit radiometric resolution and lower accuracy in exterior orientation. Steep slopes and mountainous areas often experience strong shadows, overexposed photographs on snow-covered surfaces, and clouds over mountain tops, all affecting image-matching results and vertical accuracy, and increasing noise in the DSMs.

Comparing the agreement between manual stereo measurements and the historical DSM of epoch 1, the closed forest land cover class shows the largest bias among all classes. However, similar patterns are visible when comparing manual stereo

measurements with a DSM from images acquired by a modern near-infrared Leica ADS Sensor with a GSD of 0.5 m (Ginzler et al., 2015). Ginzler et al. (2015) achieved median values of -0.34 m (coniferous) and -0.79 m (deciduous), with NMAD values in the same range as in this study. Compared to this study, the greater bias in the historical data could be due to the more challenging visual capture of canopy objects in manual stereo measurements on 8-bit panchromatic images. Also, the measurement was only performed on one stereo model, while the DSM in this study was created from the fusion of several overlapping pairs. All other land cover classes show median values between ~0.1 m and 0.7 m and NMAD values between ~1 m and 1.5 m in both studies.

#### 4.3 Challenges of image processing and limitations of our dataset

Challenges in working with airborne historical aerial images can include difficulties accessing the archive, the high cost of images, deteriorated film negatives and the poor availability of metadata such as exterior and interior orientation. In Switzerland, swisstopo provides free access to a comprehensive archive of scanned historical aerial images covering the entire country, along with calibration protocols and exterior orientation parameters for each image, essential for photogrammetric processing. However, the orientation accuracy of historical images varies between epochs, requiring a vertical correction of the DSMs due to offsets of several metres. Often, historical images lack calibration protocols and exterior orientation information, requiring ground control points to calculate the camera location. This has led the scientific community to adopt 'structure from motion' photogrammetric approaches for processing historical aerial images (e.g., Muhammed et al., 2023), as these approaches do not require approximated values, such as camera calibration information. Additionally, pipelines have been developed to minimise the effort of collecting GCPs (e.g., Knuth et al., 2023).

To handle countrywide datasets acquired over three decades, the processing of approximately 32,000 images, as well as the post-processing, including the vertical correction of about 20,000 stereo footprint DSMs, was done at the map sheet level. Vertical correction was required to minimise offsets caused by an inaccurate exterior orientation of the images (see section

Vertical correction was required to minimise offsets caused by an inaccurate exterior orientation of the images (see section 2.2.2). Each corrected map sheet DSM was merged without further consideration of the edges of adjacent map sheets, potentially creating small jumps at the edges. These jumps are negligible at the country scale, but further co-registration should be considered for local and catchment studies involving more than one map sheet.

Another challenge of historical black-and-white imagery with 8-bit radiometric resolution is oversaturation in snow-covered or heavily illuminated areas, leading to no or erroneous image-matching results, particularly in mountainous regions. This is evident in the completeness results for points classified as glacial and perpetual snow (see section 3.2). Therefore, for studies

evident in the completeness results for points classified as glacial and perpetual snow (see section 3.2). Therefore, for studies related to glaciers and snow, the noise and the voids in the generated DSMs must be addressed with proper void filling and filtering. We used a simple TIN interpolation to fill the voids, providing a binary mask indicating interpolated areas, which can be used to remove these areas for further analysis. For glaciological studies or applications requiring precise dates, we do not have the exact information on the dates of each DSM/pixel, but we provide the year of the survey campaign per map sheet.

### 5 Data availability

467

474

489

490

Datasets can be accessed from EnviDat (<a href="https://doi.org/10.16904/envidat.528">https://doi.org/10.16904/envidat.528</a>, Marty et al., 2024). The following files are available for the four epochs: countrywide digital surface model (DSM), hillshaded DSM, and vegetation height models (VHMs). A metadata shapefile is provided with information about the acquisition year of the photographs used here; the geometry corresponds to the 1:25,000 map sheets used during this study. In addition, a binary raster is provided indicating successfully matched pixels (1) and interpolated pixels (0), and a non-vegetation mask raster 'TLM\_Vegetation\_mask' is provided, indicating vegetated areas (1) and non-vegetated areas (0). All the raster files are provided as GeoTIFF files.

#### 6 Conclusions

- 475 Millions of aerial photographs dating from the First World War to the early 2000s represent an enormous, yet largely untapped, 476 resource for geoscientists, with significant potential for documenting and quantifying surface changes over the last century. In 477 this study, we used freely available historical stereo images covering the whole of Switzerland, processed using 478 photogrammetric software. These images were provided with both exterior and interior orientation, allowing us to derive four 479 countrywide DSMs at a 1 m spatial resolution across four epochs, with survey campaigns spanning approximately seven years. 480 Our developed workflow achieved meter to sub-meter accuracy and high completeness of the DSMs in nearly all regions of 481 Switzerland, demonstrating the feasibility of capturing continuous surface change patterns at a high spatial resolution over 482 different land cover classes. The vertical accuracy (NMAD) in areas below 2000 m a.s.l. and with a slope of less than 20° 483 ranges from 1.57 to 2.06 times the GSD (on average 0.35 m). However, lower completeness and increased noise were present 484 in snow-covered areas, due to image saturation and reduced performance of the image-matching algorithm in these areas. As 485 our study was conducted as part of the Swiss NFI, we also generated four countrywide VHMs using an available countrywide 486 DTM. These VHMs have been used to quantify forest changes (Ginzler et al., 2021) and monitor above-ground biomass (Price 487 et al., 2020). The high consistency of the VHMs indicates their potential for future research into forest ecosystem dynamics, 488 services and management.
- our understanding of surface changes and related processes.

  Finally, this study highlights the importance of recognising the value of historical aerial imagery datasets. We urge mapping agencies, governmental authorities and military services to unlock these archives and make them freely accessible online. The creation of countrywide historical aerial image DSMs is feasible only when such data is readily available, as demonstrated by the open access provided by swisstopo in Switzerland.

Future work can build upon these datasets by integrating modern data to extend the observation period, thereby enhancing the

detection of climate signals. Additionally, refining time series methods for very-high-resolution datasets will further improve

## 496 Appendix A

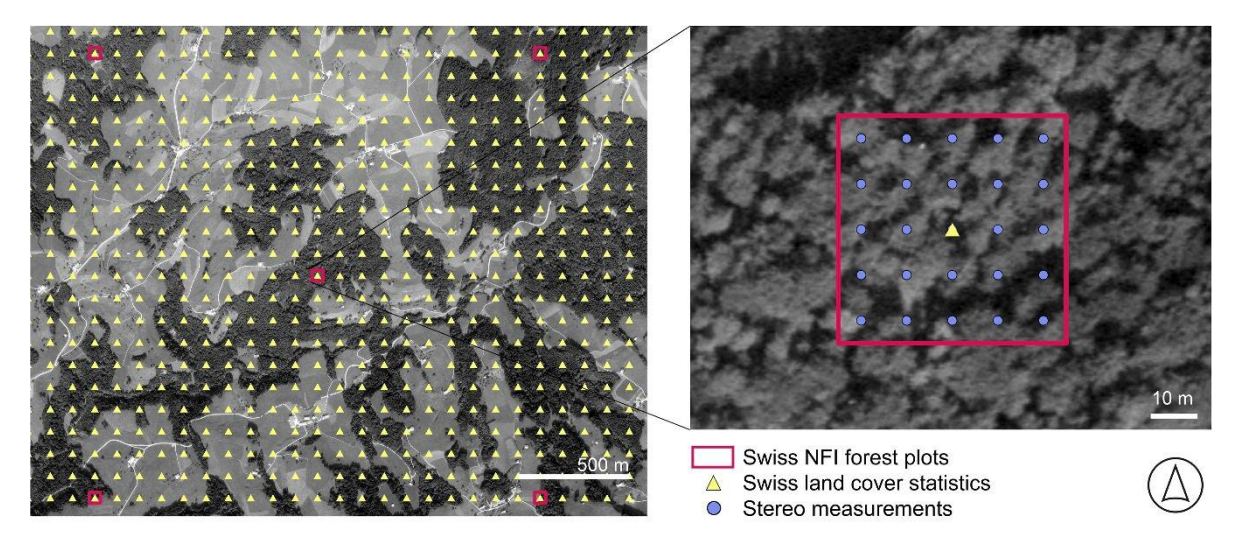


Figure A1: Illustration of the distribution of the Swiss land cover statistic points and the Swiss National Forest Inventory (NFI) forest plots with the stereo measurements. The background is the generated orthophoto from the first epoch (1979–1985).

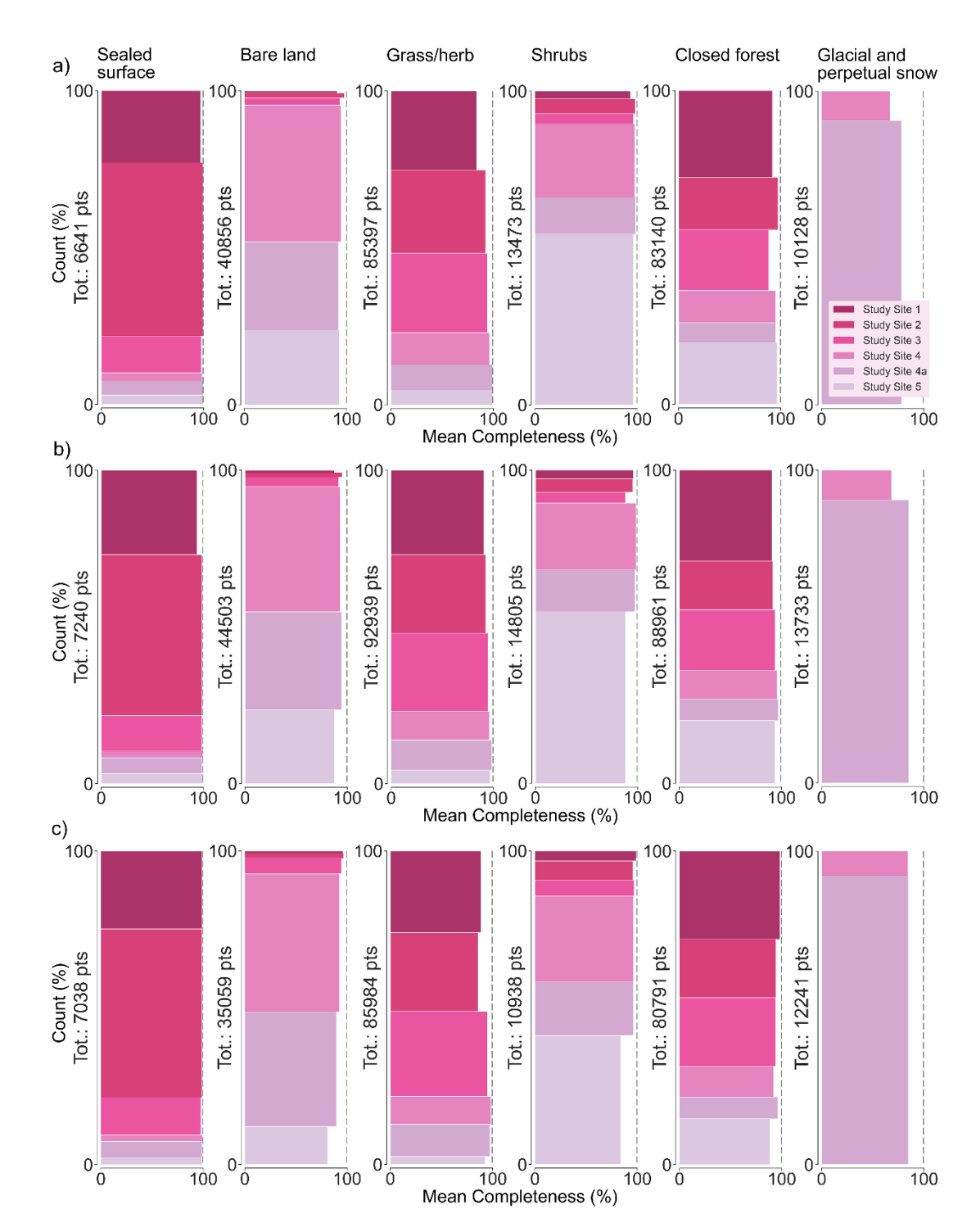


Figure A2: Distribution of the mean completeness values, as percentages, for (a) epoch 2, (b) epoch 3, and (c) epoch 4, across the six study sites and the six land cover classes – sealed surface, bare land, grass/herb, shrub, closed forest, and glacial and perpetual snow. The last class is only present in study sites 4, 4a and 5.

Table A1: Mean completeness values (as percentages) for each epoch over the six study sites, and for the six land cover classes. For each class, the number of points used to assess the accuracy is provided. n.a. indicates not available.

95 98 97 99 00	Count (No.)  1312 3416 726 173 284 190	Mean (%)  84  86  91  95  94  94	Count (No.)  221 565 1172 19892 12759 9045	Mean (%) 53 58 74 99 91	Count (No.)  17428 19879 20202 8785	Mean (%) 87 92 94	Count (No.)  286 586 409	Mean (%)  84 93	Count (No.) 17899 12254	Mean (%) n.a. n.a.	Count (No.) n.a. n.a.
98 97 99 99 .00	3416 726 173 284 190	86 91 95 94 94	565 1172 19892 12759	58 74 99	19879 20202	92	586	93			
98 97 99 99 .00	3416 726 173 284 190	86 91 95 94 94	565 1172 19892 12759	58 74 99	19879 20202	92	586	93			
97 99 99 00	726 173 284 190	91 95 94 94	1172 19892 12759	74 99	20202				12254	n.a.	n o
99 99 .00	173 284 190	95 94 94	19892 12759	99		94	400				11.d.
99 .00 97	284 190 1526	94 94	12759		8785		409	88	14877	n.a.	n.a.
.00 97	190 1526	94		91		99	3244	96	8496	51	1543
97	1526		9045		8119	98	1838	98	5346	64	9774
				99	3550	95	7125	98	15193	82	18
99		90	287	84	21520	93	331	92	22974	n.a.	n.a.
,,	3669	97	606	93	22699	98	646	97	13934	n.a.	n.a.
98	776	93	956	94	21609	96	434	88	16075	n.a.	n.a.
99	176	94	17811	96	8638	98	3139	95	8477	67	951
.00	296	92	11497	99	7163	98	1593	95	5287	78	9155
.00	198	93	9699	99	3768	96	7330	97	16393	76	22
94	1947	87	342	91	24952	96	408	91	25816	n.a.	n.a.
99	3718	95	618	92	23317	95	639	92	13841	n.a.	n.a.
98	819	91	1400	95	23259	88	514	94	17229	n.a.	n.a.
99	163	93	17761	96	8437	98	3158	96	8239	68	1312
99	360	94	13907	98	8868	98	1964	97	6060	85	12399
.00	233	87	10475	97	4106	88	8122	94	17776	87	22
	200	0,7	10.70	,	.100		0122	, .	1,,,,	0,	
99	1748	96	281	89	22408	99	348	98	22718	n.a.	n.a.
99	3784	97	560	86	21622	96	670	94	15078	n.a.	n.a.
00	840	94	1715	95		97	553	94	17637	n.a.	n.a.
98											953
98 99 99											11283 5
99		3784 840 147	3784 97 840 94 147 93 365 90	3784 97 560 840 94 1715 147 93 15428 365 90 12840	3784 97 560 86 840 94 1715 95 147 93 15428 98 365 90 12840 97	3784 97 560 86 21622 840 94 1715 95 23288 147 93 15428 98 7680 365 90 12840 97 8811	3784 97 560 86 21622 96 840 94 1715 95 23288 97 147 93 15428 98 7680 96 365 90 12840 97 8811 96	3784 97 560 86 21622 96 670 840 94 1715 95 23288 97 553 147 93 15428 98 7680 96 3008 365 90 12840 97 8811 96 1862	3784 97 560 86 21622 96 670 94 840 94 1715 95 23288 97 553 94 147 93 15428 98 7680 96 3008 92 365 90 12840 97 8811 96 1862 96	3784 97 560 86 21622 96 670 94 15078 840 94 1715 95 23288 97 553 94 17637 147 93 15428 98 7680 96 3008 92 7927 365 90 12840 97 8811 96 1862 96 5623	3784 97 560 86 21622 96 670 94 15078 n.a. 840 94 1715 95 23288 97 553 94 17637 n.a. 147 93 15428 98 7680 96 3008 92 7927 85 365 90 12840 97 8811 96 1862 96 5623 85

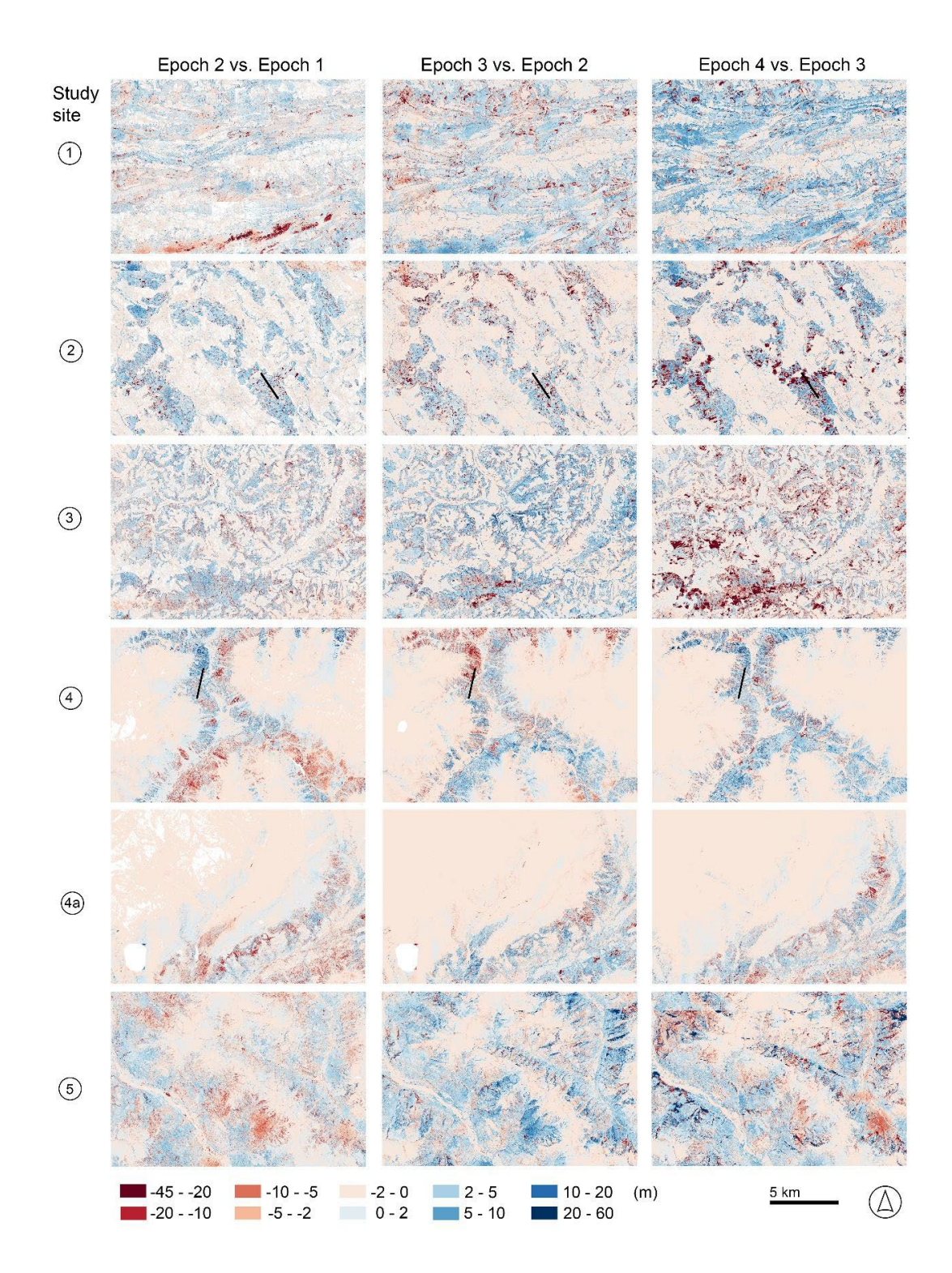


Figure A3: The height difference between the vegetation height models (VHM) of consecutive epochs for each study site (1–5). The black line in study sites 2 and 4 indicates the location of the profile shown in Figure 10.

511 **Supplement** 512 No supplemental material. 513 **Author Contributions** 514 MM and CG designed the study. MM processed and generated all the data. LP and MM analysed the dataset. LP prepared all 515 the figures and tables. LP and MM wrote the manuscript. All authors contributed to the discussion and editing of the text. 516 **Competing interests** 517 The authors declare that they have no conflicts of interest. 518 Acknowledgements 519 This study was supported by the Swiss National Forest Inventory (NFI). We thank the Federal Statistical Office FSO and the 520 Federal Office of Topography swisstopo for providing access to the historical photographs. We are grateful to Holger Heisig 521 (swisstopo) for the successful semi-automatic orientation of thousands of historical images and fruitful and interesting 522 discussions about this source of data and to Dr Melissa Dawes for professional language editing. 523 **Funding** 524 This study was carried out in the framework of the Swiss National Forest Inventory (NFI), a cooperative effort between the 525 Swiss Federal Institute for Forest, Snow and Landscape Research (WSL) and the Swiss Federal Office for the Environment 526 (FOEN). 527 References 528 Abegg, M., Bösch, R., Kükenbrink, D., and Morsdorf, F.: Tree volume estimation with terrestrial laser scanning—testing for 529 bias in a 3D virtual environment, Agric. For. Meteorol., 331, 109348, https://doi.org/10.1016/j.agrformet.2023.109348, 2023. 530 531 Belart, J.M., Magnússon, E., Berthier, E., Gunnlaugsson, Á.Þ., Pálsson, F., Aðalgeirsdóttir, G., Jóhannesson, T., Thorsteinsson, 532 T., and Björnsson, H.: Mass balance of 14 Icelandic glaciers, 1945–2017: spatial variations and links with climate, Front. Earth 533 Sci., 8, 163, https://doi.org/10.3389/feart.2020.00163, 2020.

- Berveglieri, A., Imai, N.N., Tommaselli, A.M., Casagrande, B. and Honkavaara, E.: Successional stages and their evolution
- 536 in tropical forests using multi-temporal photogrammetric surface models and superpixels, ISPRS-J. Photogramm. Remote
- 537 Sens., 146, 548-558, https://doi.org/10.1016/j.isprsjprs.2018.11.002, 2018.

- 539 Berveglieri, A., Tommaselli, A.M.G., Imai, N.N., Ribeiro, E.A.W., Guimaraes, R.B. and Honkavaara, E.: Identification of
- 540 successional stages and cover changes of tropical forest based on digital surface model analysis, IEEE J. Sel. Top. Appl. Earth
- 541 Obs. Remote Sens., 9(12), 5385-5397, https://doi.org/10.1109/JSTARS.2016.2606320, 2016.

542

- 543 BFS. Bundesamt für Statistik, Arealstatistik Schweiz Nomenklatur 2004.
- 544 <a href="https://www.bfs.admin.ch/bfs/de/home/statistiken/raum-umwelt/nomenklaturen/arealstatistik.html">https://www.bfs.admin.ch/bfs/de/home/statistiken/raum-umwelt/nomenklaturen/arealstatistik.html</a>, last access: 29 August
- 545 2024.

546

- Bolles, K.C. and Forman, S.L.: Evaluating landscape degradation along climatic gradients during the 1930s dust bowl drought
- 548 from panchromatic historical aerial photographs, United States Great Plains. Front. Earth Sci., 6, 153,
- 549 https://doi.org/10.3389/feart.2018.00153, 2018.

550

- Bożek, P., Janus, J. and Mitka, B.: Analysis of changes in forest structure using point clouds from historical aerial photographs,
- Remote Sens., 11(19), p.2259, https://doi.org/10.3390/rs11192259, 2019.

553

- 554 Cusicangui, D., Rabatel, A., Vincent, C., Bodin, X., Thibert, E., and Francou, B.: Interpretation of volume and flux changes
- of the Laurichard rock glacier between 1952 and 2019, French Alps, J. Geophys. Res. Earth Surf., 126(9), p.e2021JF006161,
- 556 https://doi.org/10.1029/2021JF006161, 2021.

557

- 558 DeVenecia K., Walker S, and Bingcai, Z.: New Approaches to Generating and Processing High Resolution Elevation Data
- with Imagery, Photogrammetric Week '07, 297-308, Wichmann Verlag, Heidelberg, 2007.

560

- Denzinger, F., Machguth, H., Barandun, M., Berthier, E., Girod, L., Kronenberg, M., Usubaliev, R., and Hoelzle, M.: Geodetic
- 562 mass balance of Abramov Glacier from 1975 to 2015, J. Glaciol., 67(262), 331-342, http://doi.org/10.1017/jog.2020.108,
- 563 2021.

564

- 565 Fleischer, F., Haas, F., Piermattei, L., Pfeiffer, M., Heckmann, T., Altmann, M., Rom, J., Stark, M., Wimmer, M.H., Pfeifer,
- N., and Becht, M.: Multi-decadal (1953–2017) rock glacier kinematics analysed by high-resolution topographic data in the
- 567 upper Kaunertal, Austria, Cryosphere, 15(12), 5345-5369, https://doi.org/10.5194/tc-15-5345-2021, 2021.

- 569 Geyman, E.C., J. J. van Pelt, W., Maloof, A.C., Faste Aas, H., and Kohler, J.: Historical glacier change on Svalbard predicts
- doubling of mass loss by 2100, Nature, 601, 374–379, https://doi.org/10.1038/s41586-021-04314-4, 2022.

- 572 Ginzler, C. and Hobi, M.L.: Countrywide stereo-image matching for updating digital surface models in the framework of the
- 573 Swiss National Forest Inventory, Remote Sens., 7, 4343–4370, https://doi.org/10.3390/rs70404343, 2015.

574

- 575 Ginzler, C., Price, B., Weber, D., Hobi, M., and Marty, M.: Dynamik der Vegetationshöhen im Schweizer Wald, Swiss Forestry
- 576 J., 172(5), 310-317, https://doi.org/10.3188/szf.2021.0310, 2021.

577

- 578 Gomez, C., Hayakawa, Y., and Obanawa, H.: A study of Japanese landscapes using structure from motion derived DSMs and
- 579 DEMs based on historical aerial photographs: New opportunities for vegetation monitoring and diachronic geomorphology,
- 580 Geomorphology, 242, 11-20, https://doi.org/10.1016/j.geomorph.2015.02.021, 2015.

581

- Heisig, H. and Simmen, J.L.: Re-engineering the past: countrywide geo-referencing of archival aerial imagery, J. Photogramm.
- 583 Remote Sens. Geoinf. Sci., 89(6), 487-503, https://doi.org/10.1007/s41064-021-00162-z, 2021.

584

- 585 Höhle, J. and Höhle, M.: Accuracy assessment of digital elevation models by means of robust statistical methods, ISPRS-J.
- 586 Photogramm. Remote Sens., 64(4), 398-406, https://doi.org/10.1016/j.isprsjprs.2009.02.003, 2009.

587

- Hufkens, K., de Haulleville, T., Kearsley, E., Jacobsen, K., Beeckman, H., Stoffelen, P., Vandelook, F., Meeus, S., Amara,
- M., Van Hirtum, L., and Van den Bulcke, J.: Historical aerial surveys map long-term changes of forest cover and structure in
- 590 the Central Congo Basin, Remote Sens., 12(4), 638, https://doi.org/10.3390/rs12040638, 2020.

591

- Hudak, A.T. and Wessman, C.A.: Textural analysis of historical aerial photography to characterise woody plant encroachment
- 593 in South African Savanna, Remote Sens. Environ., 66(3), 317-330, https://doi.org/10.1016/S0034-4257(98)00078-9, 1998.

594

- Kadmon, R. and Harari-Kremer, R.: Studying long-term vegetation dynamics using digital processing of historical aerial
- 596 photographs, Remote Sens. Environ., 68(2), 164-176, https://doi.org/10.1016/S0034-4257(98)00109-6, 1999.

597

- Knuth, F., Shean, D., Bhushan, S., Schwat, E., Alexandrov, O., McNeil, C., Dehecq, A., Florentine, C., and O'Neel, S.:
- 599 Historical Structure from Motion (HSfM): Automated processing of historical aerial photographs for long-term topographic
- 600 change analysis, Remote Sens, Environ, 285, 113379, https://doi.org/10.1016/j.rse.2022.113379, 2023.

- Korsgaard, N.J., Nuth, C., Khan, S.A., Kjeldsen, K.K., Bjørk, A.A., Schomacker, A., and Kjær, K.H.: Digital elevation model
- and orthophotographs of Greenland based on aerial photographs from 1978–1987, Sci. Data, 3, 160032,
- 604 https://doi.org/10.1038/sdata.2016.32, 2016.

- Kulha, N., Pasanen, L., and Aakala, T.: How to calibrate historical aerial photographs: a change analysis of naturally dynamic
- 607 boreal forest landscapes, Forests, 9(10), 631, https://doi.org/10.3390/f9100631, 2018.

608

- Kupidura, P., Osińska-Skotak, K., Lesisz, K., and Podkowa, A.: The efficacy analysis of determining the wooded and shrubbed
- area based on archival aerial imagery using texture analysis, ISPRS Int. J. Geo-Inf., 8(10), 450,
- 611 https://doi.org/10.3390/jigi8100450, 2019.

612

- Marty. M., Piermattei, L., Ginzler, C., and Waser, L.T..: Countrywide DSM and VHM from historical aerial images, Envidar
- 614 [data set], <a href="https://doi.org/10.16904/envidat.528">https://doi.org/10.16904/envidat.528</a>, 2024.

615

- Magnússon, E., Muñoz-Cobo Belart, J., Pálsson, F., Ágústsson, H., and Crochet, P.: Geodetic mass balance record with
- 617 rigorous uncertainty estimates deduced from aerial photographs and lidar data case study from Drangajökull ice cap, NW
- 618 Iceland, Cryosphere, 10(1), 159-177, https://doi.org/10.5194/tc-10-159-2016, 2016.

619

- Micheletti, N., Lane, S.N., and Chandler, J.H.: Application of archival aerial photogrammetry to quantify climate forcing of
- delight alpine landscapes, Photogram, Rec., 30, 143-165, https://doi.org/10.1111/phor.12099, 2015.

622

- Morgan, J.L. and Gergel, S.E.: Quantifying historic landscape heterogeneity from aerial photographs using object-based
- 624 analysis, Landscape Ecol., 25, 985-998, https://doi.org/10.1007/s10980-010-9474-1, 2010.

625

- Muhammed, M.A., Hailu, B.T., Miehe, G., Wraase, L., Nauss, T. and, Zeuss, D.: High-resolution digital elevation models and
- orthomosaics generated from historical aerial photographs (since the 1960s) of the Bale Mountains in Ethiopia, Earth Syst.
- 628 Sci. Data, 15(12), 5535-5552, https://doi.org/10.5194/essd-15-5535-2023, 2023.

629

- 630 Nebiker, S., Lack, N., and Deuber, M.: Building change detection from historical aerial photographs using dense image
- matching and object-based image analysis, Remote Sens., 6(9), 8310-8336, https://doi.org/10.3390/rs6098310, 2014.

- Nurminen, K., Litkey, P., Honkayaara, E., Vastaranta, M., Holopainen, M., Lyvtikäinen-Saarenmaa, P., Kantola, T., and
- 634 Lyytikäinen, M.: Automation aspects for the georeferencing of photogrammetric aerial image archives in forested scenes,
- Remote Sens., 7(2), 1565-1593, https://doi.org/10.3390/rs70201565, 2015.

- 637 Peppa, M.V., Mills, J.P., Fieber, K.D., Havnes, I., Turner, S., Turner, A., Douglas, M., and Bryan, P.G.: Archaeological feature
- detection from archive aerial photography with a SfM-MVS and image enhancement pipeline, Int. arch.
- 639 Photogramm. Remote Sens. Spat. Inf. Sci., 42, 869-875, https://doi.org/10.5194/isprs-archives-XLII-2-869-2018, 2018.

640

- Piermattei, L., Heckmann, T., Betz-Nutz, S., Altmann, M., Rom, J., Fleischer, F., Stark, M., Haas, F., Ressl, C., Wimmer,
- 642 M.H., and Pfeifer, N.: Evolution of an Alpine proglacial river during 7 decades of deglaciation, Earth Surf. Dyn., 11(3), 383-
- 643 403, https://doi.org/10.5194/esurf-11-383-2023, 2023.

644

- Piermattei, L., Marty, M., Ginzler, C., Pöchtrager, M., Karel, W., Ressl, C., Pfeifer, N., and Hollaus, M.: Pléiades satellite
- 646 images for deriving forest metrics in the Alpine region, Int. J. Appl. Earth Obs. Geoinf., 80, 240-256,
- 647 https://doi.org/10.1016/j.jag.2019.04.008, 2019.

648

- Price, B., Waser, L.T., Wang, Z., Marty, M., Ginzler, C. and Zellweger, F.: Predicting biomass dynamics at the national extent
- from digital aerial photogrammetry, Int. J. Appl. Earth Obs. Geoinf., 90, 102116, https://doi.org/10.1016/j.jag.2020.102116,
- 651 2020.

652

- Risbøl, O., Briese, C., Doneus, M., and Nesbakken, A.: Monitoring cultural heritage by comparing DEMs derived from
- 654 historical aerial photographs and airborne laser scanning, J. Cult. Herit., 16(2), 202-209,
- 655 https://doi.org/10.1016/j.culher.2014.04.002, 2015.

656

- 657 Schwat, E., Istanbulluoglu, E., Horner-Devine, A., Anderson, S., Knuth, F., and Shean, D.: Multi-decadal erosion rates from
- 658 glacierized watersheds on Mount Baker, Washington, USA, reveal topographic, climatic, and lithologic controls on sediment
- 659 yields, Geomorphology, 438, 108805, https://doi.org/10.1016/j.geomorph.2023.108805, 2023.

660

- 661 Swisstopo, swissALTI3D version 2017: https://backend.swisstopo.admin.ch/fileservice/sdweb-docs-prod-swisstopoch-
- 662 files/files/2023/11/14/cf4990a1-6bfb-4331-b990-a894d686266e.pdf, last access: 29 August 2024, 2017.

663

- 664 Swisstopo geodetic points: https://opendata.swiss/en/dataset/lagefixpunkte-lfp1-landesvermessung, last access: 29 August
- 665 2024, 2023.

666

- 667 Swisstopo, aerial photographs: https://www.swisstopo.admin.ch/en/analogue-aerial-photographs, last access: 29 August 2024.
- 668 2024a.

- 670 Swisstopo, National Map 1:25'000: <a href="https://www.swisstopo.admin.ch/en/national-map-1-25000">https://www.swisstopo.admin.ch/en/national-map-1-25000</a>, last access: 29 August 2024,
- 671 2024b.

- 673 Swisstopo, swissALTI3D technical information: <a href="https://www.swisstopo.admin.ch/en/height-model-swissalti3d">https://www.swisstopo.admin.ch/en/height-model-swissalti3d</a>, last access: 29
- 674 August 2024, 2024c.

675

- 676 Swisstopo, The topographic Landscape Model TLM: https://www.swisstopo.admin.ch/en/information-topographic-landscape-
- 677 model, last access: 29 August 2024, 2024d.

678

- Vastaranta, M., Niemi, M., Wulder, M.A., White, J.C., Nurminen, K., Litkey, P., Honkavaara, E., Holopainen, M., and Hyyppä,
- 680 J.: Forest stand age classification using time series of photogrammetrically derived digital surface models, Scand. J. For. Res.,
- 681 31(2), 194-205, https://doi.org/10.1080/02827581.2015.1060256, 2016.

682

- Véga, C. and St-Onge, B.: Height growth reconstruction of a boreal forest canopy over a period of 58 years using a combination
- of photogrammetric and lidar models, Remote Sens. Environ., 112(4), 1784-1794, https://doi.org/10.1016/j.rse.2007.09.002,
- 685 2008.

686

- Wang, Z., Ginzler, C., Eben, B., Rehush, N., and Waser, L.T.: Assessing changes in mountain treeline ecotones over 30 years
- using CNNs and historical aerial images, Remote Sens., 14, 2135, https://doi.org/10.3390/rs14092135, 2022.

689

- Waser, L.T., Baltsavias, E., Ecker, K., Eisenbeiss, H., Ginzler, C., Küchler, M., Thee, P., and Zhang, L.: High-resolution digital
- surface models (DSMs) for modelling fractional shrub/tree cover in a mire environment, Int. J. Remote Sens., 29(5), 1261-
- 692 1276, https://doi.org/10.1080/01431160701736422, 2008a.

693

- Waser, L.T., Baltsavias, E., Ecker, K., Eisenbeiss, H., Feldmeyer-Christe, E., Ginzler, C., and Zhang, L.: Assessing changes
- of forest area and shrub encroachment in a mire ecosystem using digital surface models and CIR aerial images, Remote Sens.
- 696 Environ., 112(5), 1956-1968, https://doi.org/10.1016/j.rse.2007.09.015, 2008b.

697

- Waser, L.T., Fischer, C., Wang, Z., and Ginzler, C.: Wall-to-wall forest mapping based on digital surface models from image-
- 699 based point clouds and a NFI forest definition, Forests, 6, 4510–4528, https://doi.org/10.3390/f6124386, 2015.

700701